https://doi.org/10.5194/egusphere-2026-5958
Preprint. Discussion started: 3 November 2026
© Author(s) 2026. CC BY 4.0 License.

Terrestrial Ecosystem Model in R (TEMIR) version 2.0: developing a crop model to simulate the response of maize and soybean to elevated CO_2 and O_3 concentrations

Jacky Y. S. Pang[1,2], Aditya Abha Singh[3,4], Shashi Bhushan Agrawal[4], Syam Chintala[5], Zhaozhong Feng[6], Amos P. K. Tai[1,2,7]

[1]Department of Earth and Environmental Sciences, The Chinese University of Hong Kong, Hong Kong
[2]Institute of Environment, Energy and Sustainability, The Chinese University of Hong Kong, Hong Kong
[3]Department of Botany, University of Lucknow, Lucknow, India
[4]Laboratory of Air Pollution and Global Climate Change, Department of Botany, Institute of Science, Banaras Hindu University, Varanasi 221005, India
[5]Department of Civil Engineering, Indian Institute of Technology Hyderabad, Telangana, India
[6]School of Ecology and Applied Meteorology, Nanjing University of Information Science and Technology, Nanjing, 210044, China
[7]State Key Laboratory of Agrobiotechnology, The Chinese University of Hong Kong, Hong Kong

Correspondence to: Amos P. K. Tai (amostai@cuhk.edu.hk)

Abstract.

Surface ozone (O_3) pollution threatens global crop production, and future projections indicate severe risks to regional food security under worsening air pollution. Concurrently, rising atmospheric carbon dioxide (CO_2) can partially offset ozone damage by stimulating carbon assimilation and reducing stomatal ozone uptake. Here, a process-based crop module is integrated into the offline Terrestrial Ecosystem Model in R (TEMIR), enabling simulations of crop growth and yield under varying CO_2 and ozone concentrations at site to global scales. We describe the module structure, evaluate performance against benchmark flux-tower observations for maize and soybean, and calibrate ozone damage parameters using gas-exchange data from field elevated CO_2 or ozone fumigation experiments. For soybean, with ozone damage parameters calibrated using SoyFACE data, TEMIR reproduces ozone-induced relative yield loss with a mean error of 5 percentage points, substantially improving upon uncalibrated simulations (30 percentage points error), with photosynthetic declines closely mirroring yield reductions. In contrast for maize, simulations with parameters calibrated to leaf-level gas exchange overestimate relative biomass loss by 30 percentage points at 100 ppb ozone. Reconciling simulated biomass with observations requires reducing photosynthetic ozone sensitivity by 66–75%, demonstrating that maize biomass and yield are buffered against leaf-level photosynthetic impairment. These divergent responses across maize and soybean indicate that modelers must select ozone-sensitivity parameters aligned with specific research objectives (e.g., yield estimation versus carbon- and water-flux assessments). Ultimately, the TEMIR crop module enables comprehensive assessments of agricultural impacts across future climate and pollution scenarios, particularly in pollution hotspots such as the US, China, and India. By bridging physiological

https://doi.org/10.5194/egusphere-2026-5958
Preprint. Discussion started: 3 November 2026
© Author(s) 2026. CC BY 4.0 License.

mechanisms and agronomic productivity, this framework provides science-based evidence on the agricultural co-benefits of air quality management, advancing climate-resilient food security and Sustainable Development Goals.

1 Introduction

Global food demand is projected to increase by 35–56% by year 2050 relative to year 2010 based on different Shared Socioeconomic Pathways (SSPs) (van Dijk et al., 2021). Production of staple crops such as wheat, rice, maize, and soybean increased by ~3% per year in the 1970s, and since then the increase had gradually declined to +1.0 to +1.5% annually in the 2010s (FAO, 2017). To fulfill future food demand, food production has to overcome challenges such as the stagnation of yield growth and a deteriorating environment for growing crops. Anthropogenic activities have multiple facets influencing future food security projections, with positive influences such as technological advancements and negative influences such as land degradation impacting crop yields.

Air pollution, in particular surface ozone (O_3) pollution, is one of the largest challenges to future food security. Due to the strong oxidizing power of ozone, its uptake by plants can impair photosynthetic activities and thereby induce yield losses (e.g., Reich, 1987). It is estimated that surface ozone resulted in about 0.2–20% global loss of staple crops on average in year 2005 – 2014, which is equivalent to an economic loss of $10–63 billion USD in year 2010 (Murray et al., 2024). A similar estimation conducted by Feng et al. (2022) suggested that ozone-induced economic yield loss in East Asia alone can reach $63 billion USD in late 2010s. Surface ozone concentrations are tightly linked to the emission of ozone precursors including nitrogen oxides ($NO_x = NO_2 + NO$), carbon monoxide (CO), and volatile organic compounds (VOCs) from anthropogenic activities and natural sources. The total tropospheric ozone burden is projected to increase from 337 Tg in year 2000 to 395 Tg in year 2100 under the Representative Concentration Pathway RCP 8.5 (Young et al., 2013). India and China are the two most populous countries in the world and therefore also have a large food demand, but at the same time both countries face severe challenges in ozone pollution that imposes stress on crop growth. Model simulations conducted by Bhattarai et al. (2024) suggested that in the Shared Socioeconomic Pathways (SSPs) SSP3 and SSP5, where the mitigation of climate impacts is challenging (O'Neill et al., 2017), China (10–20%) and India (25–40%) are regions that have the highest increase in the Maximum Daily 8-Hour Average (MDA8) ozone concentration, relative to the baseline at year 2010. Avnery et al. (2011) estimated that India and China would each have an additional $1.0 billion USD equivalent loss in crop production in year 2030 relative to year 2000 due to ozone pollution. Sampedro et al. (2020) suggested that ozone-induced yield loss for staple crops in India can be tripled in year 2080 (USD $13.3 billion based on year 2015), relative to that in year 2010 ($4.1 billion USD based on year 2015).

Another facet of anthropogenic activities that influences future food production is the continuous emission of CO_2 into the atmosphere, which has positive effects on crop growth in general. The mean atmospheric CO_2 concentration is projected to reach ~500 ppm under RCP 4.5, RCP 6, and RCP 8.5 in year 2050, and around 1000 ppm under RCP 8.5 in year 2100, from

https://doi.org/10.5194/egusphere-2026-5958
Preprint. Discussion started: 3 November 2026
© Author(s) 2026. CC BY 4.0 License.

370 ppm in year 2000 (van Vuuren et al., 2011). Under elevated CO_2 concentrations, carboxylation of the photosynthetic enzyme, Rubisco, occurs more readily and enhances photosynthetic rate, especially for C_3 plants such as soybean and wheat. For C_4 plants like maize, positive effects of elevated CO_2 are smaller as CO_2 is concentrated first at the mesophyll before carboxylation. The carboxylation rate of Rubisco is therefore less dependent on the ambient CO_2 concentrations. This has been showcased in the studies of CO_2 fertilization effects with the Free-air concentration enrichment (FACE), which revealed that the saturated photosynthetic rate (A_{sat}) increases by ~40% in C_3 species and 0–20% in C_4 species at 550 ppm of CO_2 relative to 370 ppm (Ainsworth and Long, 2005). Apart from the direct increase in photosynthetic rate, elevated CO_2 reduces stomatal conductance (g_s) and thus ozone uptake. FACE experiments suggested that g_s of both C_3 and C_4 species is reduced by 20–40% under elevated CO_2, accompanied by reduced transpiration water loss and enhanced water use efficiency (Ainsworth and Long, 2005).

To investigate the joint effects of elevated CO_2 and O_3 on crop production, we implemented a crop model into the base model of Terrestrial Ecosystem Model in R (TEMIR) (Tai et al., 2024). TEMIR is an offline vegetation model designed to be input-compatible with the GEOS-Chem chemical transport model to examine various facets of biosphere-atmosphere interactions. For instance, hourly ozone output from GEOS-Chem in different emission scenarios can be readily used in TEMIR to investigate the impacts of ozone on vegetation productivity, which is shown in the study of the impacts of ozone changes on vegetation productivity via stratospheric aerosol injection (Moch et al., 2023). The newly implemented crop model calculates vegetation carbon budgets based on phenology. It was first used in a comparison between the ozone-induced yield losses estimated with conventional empirically based metrics (e.g., AOT40, POD_3) and those simulated by a mechanistic crop model (Tai et al., 2021).

The first aim of this paper is to provide a comprehensive description of the crop model, and to demonstrate its ability to simulate maize and soybean growth under a stress-free ambient environment. The model was evaluated against two eddy covariance measurement sites, which have a set of carbon budget observations such as gross primary production (GPP) and biomass. The second aim of this paper is to calibrate a set of ozone damage parameters to simulate ozone damage induced on two specific crops, maize and soybean. Two ozone damage schemes were implemented in the base TEMIR model: one is based on Sitch et al. (2007) where ozone damage is based on the hourly stomatal ozone uptake flux and parameters were calibrated to yield loss observations (e.g., Pleijel et al., 2004); the other is based on Lombardozzi et al. (2012b, 2015) where damage is based on the long-term cumulative stomatal ozone uptake and parameters were calibrated to gas-exchange rate loss observations. These schemes have been used for the assessment of the changes in global terrestrial carbon budgets and vegetation-atmosphere coupling under ozone damage, whereby multiple plant species are usually lumped into a single plant functional group such as C_3 grasses for simplicity (Sadiq et al., 2017; Oliver et al., 2018; Zhou et al., 2018; Franz and Zaehle, 2021; Zhu et al., 2022). Therefore, calibration of ozone sensitivity parameters of individual staple crops enables a more precise assessment of both local- and global-scale yield loss.

This work evolves TEMIR into a dual-purpose ecosystem and agriculture assessment platform, allowing the evaluation of ecosystem services from both natural vegetation and agroecosystems affected by climate change and environmental pollution.

https://doi.org/10.5194/egusphere-2026-5958
Preprint. Discussion started: 3 November 2026
© Author(s) 2026. CC BY 4.0 License.

Critically, this framework bypasses the need for computationally expensive, fully coupled Earth system models, which often require specialized technical expertise beyond that of stand-alone crop models and chemical transport models. This integrated capacity is highly relevant to policy assessment related to complex atmospheric management strategies, spanning from localized emissions control or land-use change to global climate intervention measures.

2 Model description

2.1 TEMIR v1.0 general description

The complete description of TEMIR v1.0 can be found in Tai et al. (2024). Briefly, it is a standalone, multi-parameterization model to simulate important canopy and ecophysiological processes that are relevant for ecosystem exchange and atmospheric chemistry. It is designed to have compatible inputs and land surface representation with the GEOS-Chem global chemical transport model. Leaf-level photosynthesis and stomatal conductance for C_3 and C_4 plants are characterized by the Farquhar Ball-Berry gas exchange model (Farquhar et al., 1980; von Caemmerer and Farquhar, 1981; Collatz et al., 1991, 1992). Vegetation canopy is stratified into two layers that make use of direct and diffuse sunlight following Dickinson (1983) and Sellers (1985). The amount of sunlight absorbed by the two layers of canopy depends on prescribed bio-physiological properties of plants such as canopy light extinction coefficient and leaf radiation reflectance, similar to the implementation of that in the Community Land Model version 4.5 (CLM4.5; Oleson et al., 2013).

2.1.1 Water limitation on plant growth and stomatal conductance

Water stress on plants is represented by the soil water stress factor (β_t) that fractionally reduces the leaf-level net photosynthetic (A'_n) rate and leaf-level stomatal conductance without water stress (g'_s) calculated from the Farquhar Ball-Berry gas exchange model (Equation 1 and 2). The value of β_t is calculated by comparing the soil water matric potential (ψ) with the PFT-specific matric potential constants at which stomatal closure (ψ_c) and stomatal opening occur (ψ_o) to the full extent (Equation 3). By default, the soil water matric potential is derived from soil water content (θ) input from reanalysis products (e.g., GMAO, 2015) or site measurements, together with soil hydraulic properties including the saturated soil matric potential (ψ_{sat}), saturated soil water content (θ_{sat}), as well as the statistical parameter B (Equation 4). Soil hydraulic properties are characterized by soil compositions (percentage of sand, slit, clay, and organic matters) and pedotransfer functions (Clapp and Hornberger, 1978; Cosby et al., 1984; Lawrence and Slater, 2008).

$A_n = A'_n(\beta_t)$	(1)
$g_s = g'_s(\beta_t)$	(2)

https://doi.org/10.5194/egusphere-2026-5958
Preprint. Discussion started: 3 November 2026
© Author(s) 2026. CC BY 4.0 License.

$\beta_t = \begin{cases} 1 & \psi > \psi_o \\ \frac{\psi-\psi_c}{\psi_o-\psi_c} & \psi_o \geq \psi \geq \psi_c \\ 0 & \psi_c > \psi \end{cases}$	(3)
$\psi = \psi_{sat}\left(\frac{\theta}{\theta_{sat}}\right)^{-B}$	(4)

2.1.2 Parameterization of ozone damage on vegetation

Ozone damage schemes following Sitch et al. (2007) (hereinafter referred to as 'Sitch scheme') and Lombardozzi et al. 2015) (hereinafter referred to as 'Lombardozzi scheme') are implemented in TEMIR, both of which model ozone damage based on the hourly effective uptake flux of ozone through the stomata (F_{O3}, in nmol O_3 m^{-2} s^{-1}) (Equation 5):

$F_{O3} = \max\left(\frac{[O_3]}{g_{ah}^{-1} + g_b^{-1} + k_{O_3} g_s^{-1}} - F_{crit}, 0\right)$	(5)

where $[O_3]$ is the hourly ground-level ozone concentration (in nmol m^{-3}); g_{ah}, g_b, g_s are the aerodynamic, boundary, and leaf-level stomatal conductance, respectively; k_{O3} = 1.67 is the ratio of the uptake resistance to that for water vapor; F_{crit} is a statistical parameter (in nmol O_3 m^{-2} s^{-1}) derived from field experiments that represent the critical level of ozone that starts damaging plants.

The two schemes differ in the calculation of the ozone impact factor (*f*) on photosynthesis and stomatal conductance (Equation 6). In the Sitch scheme, *f* is calculated with a linear equation with respect to F_{O3} at every model timestep (hourly), whereas in the Lombardozzi scheme *f* is calculated from the accumulation of the effective uptake of ozone (CUO, in mmol O_3 m^{-2} h^{-1}) (Equation 6). In some studies and documents, CUO is denoted as the phytotoxic ozone dose (POD) and the critical ozone level F_{crit} is denoted by *y* (e.g., POD_y in CLRTAP, 2023). Here we follow the notation CUO used in the Lombardozzi scheme. The accumulation of CUO starts when crops LAI reach 0.5 and ends when crops are harvested in TEMIR (Lombardozzi et al., 2012b).

$f = \begin{cases} 0 \leq b_{\text{Sitch}} - a_{\text{Sitch}} F_{O_3} \leq 1 \\ 0 \leq b_{\text{Lombardozzi}} - a_{\text{Lombardozzi}} \text{CUO} \leq 1 \end{cases}$		(6)
$\text{CUO}_t = \text{CUO}_{t-1} + 0.0036 F_{O_3} \times \max(1, (\frac{\text{LAI}_t - \text{LAI}_{t-1}}{\text{LAI}_{t-1}}))$	for $\text{LAI}_{t-1} > 0$	(7)

Parameter *a* is the sensitivity of plant photosynthesis and stomatal conductance to ozone; *b* is the intercept of the regression. 0.0036 is the unit conversion factor from nmol O_3 m^{-2} s^{-1} to mmol O_3 m^{-2} h^{-1} for the accumulation of CUO, and the increment of CUO is adjusted by the amount of newly grown leaves relative to the amount of old leaves to represent the lack of cumulative damage of new leaves (Equation 7). The ozone damage factor *f* is applied to the leaf-level net photosynthetic rate. In the

https://doi.org/10.5194/egusphere-2026-5958
Preprint. Discussion started: 3 November 2026
© Author(s) 2026. CC BY 4.0 License.

Lombardozzi scheme, ozone damage decouples photosynthesis and stomatal conductance from the Ball-Berry formulation (Equations 8 and 9; Lombardozzi et al., 2012b). Damage factors for stomatal conductance (f_{gs}) and photosynthesis (f_{An}) are both calculated from Equation 6 and 7 but with independently derived statistical parameters $a_{\text{Lombardozzi}}$ ($a_{\text{Lombardozzi_gs}}$ and $a_{\text{Lombardozzi_An}}$) and $b_{\text{Lombardozzi}}$ ($b_{\text{Lombardozzi_gs}}$ and $b_{\text{Lombardozzi_An}}$). In the Sitch scheme, the damage factor f only applies to photosynthesis (Equation 8). Stomatal conductance is still coupled to the ozone-damaged photosynthesis rate following the Ball-Berry formulation and the value of g_s is solved by iterating Equations 5, 6, 8 and the Ball-Berry formulation until variables $A_{n,O3}$, f_{An}, and $g_{s,O3}$ all converge.

$A_{n,O_3} = A_n(f_{A_n})$	(8)
$g_{s,O_3} = g_s(f_{g_s})$	(9)

Statistical parameters a_{Sitch} and b_{Sitch} are derived differently in the Lombardozzi scheme and in the Sitch scheme. In the Sitch scheme, parameters are calibrated for the relative reduction of biomass or crop yield to the cumulative ozone uptake, as described in Pleijel et al. (2004) and Cheesman et al. (2024). The ozone damage factor f is modeled by the hourly effective stomatal uptake and therefore follows the variation of hourly O_3 concentrations, which does not necessarily match with field observations wherein the reduction of photosynthetic rate is more sensitive to the long-term ozone exposure than short-term exposure (Betzelberger et al., 2012; Yendrek et al., 2017; Choquette et al., 2020). As a result, with the Sitch scheme a model can reproduce plant carbon budget on a monthly timescale (e.g., growing season biomass), but not necessarily the carbon budget in an hourly timescale (photosynthetic rate). This issue is apparent in the study of Leung et al. (2020), who calibrated ozone damage factor parameters based on the Sitch scheme for soybean, finding a good agreement in simulating relative yield loss and aboveground biomass under elevated ozone concentrations, but not for the early growing season LAI. The underestimation of the early growing season LAI hints at an overestimation of ozone damage during the vegetative stage when ozone damage is still not apparent. In the Lombardozzi scheme, parameters $a_{\text{Lombardozzi}}$ and $b_{\text{Lombardozzi}}$ for both A_n and g_s are derived from responses of gas-exchange rates to the cumulative stomatal ozone uptake (Lombardozzi et al., 2012a, 2013). Its formulation captures the loss of photosynthetic rate and stomatal conductance to long-term ozone exposure especially for field observations from Betzelberger et al. (2012) and Yendrek et al. (2017). Default and calibrated parameters of the Lombardozzi scheme are shown in Table 1. Details of the calibration of statistical parameters $a_{\text{Lombardozzi}}$ and $b_{\text{Lombardozzi}}$ for both A_n and g_s are shown in the Supplementary material Section S1.

https://doi.org/10.5194/egusphere-2026-5958
Preprint. Discussion started: 3 November 2026
© Author(s) 2026. CC BY 4.0 License.

Table 1. Key parameters to simulate the effect of O_3 on plant photosynthesis and stomatal conductance in the Lombardozzi scheme. [&]Sensitivity values derived based on gas-exchange measurements as intended in Lombardozzi scheme. [#]Recommended value that is calibrated to biomass and crop yield observations instead of gas-exchange measurements, see Section 5.3.

Parameters (unit)	Default (Lombardozzi et al., 2015)	Calibrated	
	'Crop and grass'	Maize	Soybean
F_{crit} (nmol O_3 m^{-2} s^{-1})	0.8	4	3
$a_{Lombardozzi_An}$ (m^2 mmol O_3^{-1})	−0.0009	−0.085 to −0.124[&] −0.02 ± 0.01[#]	−0.022 ± 0.006
$b_{Lombardozzi_An}$ (unitless)	0.8021	1	1
$a_{Lombardozzi_gs}$ (m^2 mmol O_3^{-1})	0	−0.050 ± 0.050	$-0.014^{+0.014}_{-0.006}$
$b_{Lombardozzi_gs}$ (unitless)	0.7511	1	1

2.2 Crop module description in TEMIR v2.0

In TEMIR version 2.0, a crop module for wheat, maize, and soybean has been implemented to simulate the carbon budget in plants after carbon assimilation. The crop module includes sub-modules to calculate plant total respiration, phenology, carbon allocation, and vegetation structure that mostly follow those implemented in the CLM4.5 (Drewniak et al., 2013) or the Joint-UK Land Environment Simulator (JULES) (Osborne et al., 2015). The crop module was used in previous studies (Tai et al., 2021) to simulate the impacts of O_3 and CO_2 concentrations on relative yield but its performance was not evaluated extensively in different major crop production regions. In TEMIR v2.0, various schemes in the crop module have been modified to improve its performance.

2.2.1 Crop phenology

The crop phenology sub-module determines the timing of sowing, emergence, flowering, and harvesting. Crop sowing can be prescribed or dynamically simulated, offering flexibility for both present-day simulations and future scenario simulations. For present-day simulations, crop planting can be prescribed by crop calendar datasets such as Sacks et al. (2010), or sowing records specifically for single-site simulations. In future scenario simulations that involve global warming, a dynamic crop calendar can reflect the shifts in sowing and harvesting days driven by projected temperature increases (Mourtzinis et al., 2019; Lv et al., 2020). The dynamic crop calendar in TEMIR v2.0 currently follows entirely the implementation in CLM 4.5, and future improvement of the dynamic crop model can follow for example the study by Reddy et al. (2025). After sowing, the phenology of crops is tracked by growing degree days (GDD) and development index (DVI) (Equation 10 and 11). GDD represents the cumulative heat units presented in crops, while DVI denotes the growing stage of crops with a normalized index. Both variables are updated daily in the model based on the formula:

https://doi.org/10.5194/egusphere-2026-5958
Preprint. Discussion started: 3 November 2026
© Author(s) 2026. CC BY 4.0 License.

$$\mathrm{GDD}=\begin{cases}0 & \text{for } T_{2\mathrm{m}}<T_{\mathrm{b}}\\ T_{2\mathrm{m}}-T_{\mathrm{b}} & \text{for } T_{\mathrm{b}}\le T_{2\mathrm{m}}<T_{\mathrm{o}}\\ (T_{\mathrm{o}}-T_{\mathrm{b}})\left(1-\frac{T_{2\mathrm{m}}-T_{\mathrm{o}}}{T_{\mathrm{max}}-T_{\mathrm{o}}}\right) & \text{for } T_{\mathrm{o}}\le T_{2\mathrm{m}}<T_{\mathrm{max}}\\ 0 & \text{for } T_{2\mathrm{m}}\ge T_{\mathrm{max}}\end{cases}$$	(10)
$$\mathrm{DVI}=\begin{cases}-1+\frac{\mathrm{GDD}}{\mathrm{GDD_{emer}}} & \text{for } \mathrm{GDD}<\mathrm{GDD_{emer}}\\ \frac{\mathrm{GDD}-\mathrm{GDD_{emer}}}{\mathrm{GDD_{repr}}-\mathrm{GDD_{emer}}} & \text{for } \mathrm{GDD_{emer}}\le\mathrm{GDD}<\mathrm{GDD_{repr}}\\ 1+\frac{\mathrm{GDD}-\mathrm{GDD_{repr}}}{\mathrm{GDD_{mat}}-\mathrm{GDD_{repr}}}) & \text{for } \mathrm{GDD_{repr}}\le\mathrm{GDD}<\mathrm{GDD_{mat}}\end{cases}$$	(11)

where T_{2m} is the mean daily air temperature; T_b, T_o, and T_{max} are the base, optimal, and maximum temperatures for crop growth respectively. Following the description in JULES-crop (Osborne et al., 2015), DVI values of -1, 0, 1 and 2 denote crop sowing, emergence, reaching the reproductive stage (flowering), and reaching physiological maturity respectively. GDD requirements for crop emergence, reaching the reproductive stage, and reaching physiological maturity are denoted by GDD_{emer}, GDD_{repr}, and GDD_{mat} respectively. Similar to the crop planting date, the values of GDD_{mat}, GDD_{repr}, and GDD_{emer} can either be prescribed or dynamically calculated. Dynamically calculated GDD requirements also currently follow the implementation of CLM4.5.

2.2.2 Respiration and biomass allocation

The respiration module follows the implementation in CLM 4.5, in which maintenance respiration (MR) and growth respiration (GR) are calculated. Maintenance respiration is calculated for every modeled plant component including leaves, stem, root, and reproductive part following Ryan (1991) (Equation 12). Growth respiration is the additional respiration required when plants grow in biomass, which is set to be 30% of the difference between net photosynthetic rate and total maintenance respiration for crops (Equation 13). The available carbon for biomass allocation each day (i.e., NPP) is the sum of the hourly difference between photosynthetic rate and total plant respiration (Equation 14):

$\mathrm{MR}_i=\frac{C_i}{\mathrm{CN_i}}k_{\mathrm{base}}Q^{\frac{T-20}{10}}$ $\quad i$ = leaf, stem, root, repr	(12)
$\mathrm{GR}=0.3\times\max(0,A_n-\mathrm{MR})$	(13)
$\mathrm{NPP}=max(0,\ \sum_{\mathrm{h}}(A_n-\mathrm{MR}-\mathrm{GR}))$	(14)

where C_i is the carbon content (in gC m^{-2}) in the carbon pool of plant components (leaf, stem, root, and reproductive parts); CN_i is the prescribed C:N ratio of the plant parts following values used in CLM 4.5; k_{base} is the respiration rate per unit nitrogen content at 20°C; $Q = 2$ is the sensitivity of respiration to temperature; and T (in °C) is the soil temperature at 30 cm depth for root maintenance respiration, or the 2 m air temperatures for above-ground biomass maintenance respiration.

https://doi.org/10.5194/egusphere-2026-5958
Preprint. Discussion started: 3 November 2026
© Author(s) 2026. CC BY 4.0 License.

NPP is allocated to five different carbon pools including leaf, stem, stem reserved for retranslocation, root, and the reproductive parts. The fraction of NPP that is allocated to each plant carbon pool (a_{pool}) is modeled with logistic equations following Penning de Vries et al. (1989) and JULES-crop (Osborne et al., 2015; Equation 15 to 20).

$a_{leaf} = \frac{\exp(\alpha_{leaf}+\beta_{leaf}DVI)}{\Delta}$	(15)
$a_{stem} = \frac{\exp(\alpha_{stem}+\beta_{stem}DVI)}{\Delta}\tau$	(16)
$a_{stem,resv} = \frac{\exp(\alpha_{stem}+\beta_{stem}DVI)}{\Delta}(1-\tau)$	(17)
$a_{root} = \frac{\exp(\alpha_{root}+\beta_{root}DVI)}{\Delta}$	(18)
$a_{repr} = \frac{1}{\Delta}$	(19)
$\Delta = 1 + \sum_i^{leaf,\ stem,\ root}(\exp(\alpha_i + \beta_i DVI))$	(20)

where α and β are PFT-specific parameters. The allocation scheme used in TEMIR only considers the effect of phenology. A more sophisticated variant of the logistic equations that consider the impacts of water stress, light stress, and nitrogen stress on allocation can be implemented following Peng et al. (2018) in the future. Values of α and β for maize and soybean are currently adopted from the studies conducted by Williams et al. (2017) and Leung et al. (2020), respectively, who calibrated the allocation parameters based on the observations at FLUXNET sites US-Ne1 and Ne2.

2.2.3 Leaf senescence, retranslocation of assimilated carbon, and crop yield

At the late growing stages, leaves senesce and assimilated carbon stored in leaves and stem is transferred to the reproductive parts. In CLM 4.5 and JULES-crop, leaf senescence rate is modeled following a first-order decay (CLM 4.5: 0.002 d^{-1}; JULES: 0.05 d^{-1}) of the leaf carbon pool. In TEMIR, the leaf senescence rate is modified following a power regression that can better represent the accelerating loss of the overall canopy leaves in crops during the late growing stage (Fig S4).

$\frac{dC_{leaf}}{dt} = -C_{leaf}(a_{sen}d^{b_{sen}})$ for $DVI \geq DVI_{sen}$	(21)

where d is the number of days since the start of senescence; a_{sen} and b_{sen} are crop-specific senescence parameters derived from field observations of normalized LAI and leaf biomass. An increasing senescence rate does not necessarily mean canopy leaves at later growing stages have a shorter lifetime than leaves at earlier growing stages, but indicates there is still new grown leaves to offset the senescence loss during the middle growing stages, which leads to a low loss rate in canopy leaves overall. The timing of the initial reduction in canopy leaves (DVI_{sen}) follows the calibrated values used in Williams et al. (2017) and Leung et al. (2020). Implementation of the retranslocation scheme and rate also entirely follow that in JULES-crop (Osborne et al., 2015; Williams et al., 2017; Leung et al., 2020), in which carbon from senesced leaves and stem reserve ($C_{stem,resv}$) is transported to the reproductive part (Equation 22). The carbon budget of the reproductive part is contributed by

https://doi.org/10.5194/egusphere-2026-5958
Preprint. Discussion started: 3 November 2026
© Author(s) 2026. CC BY 4.0 License.

three sources, which include the main contribution from NPP allocation, and minor contribution from the retranslocation of leaf and stem carbon.

The final crop yield (C_{harv}, in gC m^{-2}) is a fraction f_{harv} of the carbon in the reproductive part that is consumable content. In maize and soybean, f_{harv} is specifically the mass ratio of kernels to the whole ear and beans to the whole pod, respectively. The final harvested grain carbon (C_{harv}) is calculated from the carbon content in that fraction (f_{harv}, Equation 23). Values of f_{harv} for maize and soybean vary with cultivars, which are 70–90% for soybean (Ahmed et al., 2018; Gaspar et al., 2017) and 80–90% for maize (Halvorson and Johnson, 2009). They serve as uncertainties in harvest biomass observations if the harvest method (e.g., grain only, whole pod) is not explicitly specified in the experiment.

$\frac{dC_{\text{stem,resv}}}{dt} = -0.1C_{\text{stem,resv}} \quad \text{for } a_{\text{stem}} \leq 0.01$	(22)
$C_{\text{harv}} = C_{\text{repr}}(f_{\text{harv}})$	(23)

2.2.4 Vegetation structure

The vegetation structure module updates LAI, stem area index, and vegetation height daily. LAI is proportional to the amount of carbon present in the leaf carbon pool, scaled by the specific leaf area (SLA, in m^2 gC^{-1}) (Equation 24). In TEMIR, SLA is modified from the constant values adopted in CLM4.5 to reflect the responses of plant traits to the environment. Observations from Mead FLUXNET sites (Williams et al., 2017; Leung et al., 2020) and several Chinese sites (Li et al., 2023; Zhou et al., 2020) suggest SLA values for maize and soybean decrease (i.e., leaves become thicker) toward the late growing stages. SLA also responds to CO_2 and ozone concentrations as well, with decreases in SLA at elevated CO_2 (Ainsworth and Long, 2005) and increases in SLA at elevated O_3 (Betzelberger et al., 2012).

SLA is calculated following Equation 25:

$\text{LAI} = \text{SLA} \times C_{\text{leaf}}$	(24)
$\text{SLA} = \text{SLA}_{\text{base}} \times f_{\text{phen}} \times f_{\text{CO}_2} \times f_{\text{O}_3}$	(25)
$f_{\text{phen}} = \frac{(\text{DVI} + 0.06)^{\delta}}{1.06^{\delta}}$	(26)

where SLA_{base} is the SLA when DVI = 1; f_{phen} is the phenology factor such that it represents the decline in SLA at the late growing stages. The expression $\text{SLA}_{\text{base}} \times f_{\text{phen}}$ is identical to SLA in JULES (Leung et al., 2020; Osborne et al., 2015; Williams et al., 2017). Two additional expressions f_{CO2} and f_{O3} are added to represent the effects of CO_2 and O_3, respectively, but can be disabled in the simulations (i.e., f_{CO2} and $f_{O3} = 1$).

The calculation of plant height (h, in m) follows the scheme in JULES-crop, in which an allometric equation of stem carbon and crop height is established:

$h = \kappa(C_{\text{stem}})^{\lambda}$	(27)

Values of all the parameters can be found in Table S2.

https://doi.org/10.5194/egusphere-2026-5958
Preprint. Discussion started: 3 November 2026
© Author(s) 2026. CC BY 4.0 License.

3 Dataset for model validation and calibration

3.1 Crop growth under ambient environment

To evaluate the performance of the crop module to simulate crop growth under ambient conditions, FLUXNET site US-Ne2 and an Indian maize site (IN-Hyd) are selected for model validation. US-Ne2 is an irrigated maize and soybean rotation field at Mead, Nebraska, US, dedicated for the study of cropland carbon budget since year 2001. The mean growing season temperature at US-Ne2 is around 20 °C. FLUXNET data at the Mead site is a benchmark for the development of land-surface models and crop models such as JULES (Williams et al., 2017 and Leung et al., 2020) and CLM-APSIM (Peng et al., 2018). Growing seasons from the years 2001 to 2007 are evaluated, during which maize and soybeans were planted in odd and even years, respectively.

IN-Hyd is a tropical irrigated maize site located in Hyderabad, Telangana, in southern India. An eddy covariance tower has been set up at the site to measure carbon and water budgets, accompanied by ground-based measurements of LAI and biomass. TEMIR is evaluated against the growing season measurement data in the summer of 2019 from May to September (Karimindla et al., 2024), which features a growing season temperature ranging between 30 and 35 °C. Unlike temperate maize sites in the midwestern US and western Europe, which have been extensively studied (e.g., Wu et al., 2016; Williams et al., 2017), studies on tropical maize plantations with eddy covariance measurements remain scarce. Evaluation of TEMIR against observation data at IN-Hyd could provide insights into the applicability of TEMIR in simulating crop growth in diverse environments for global-scale assessments.

Eddy covariance measurement data of all FLUXNET sites are included in the FLUXNET2015 dataset (Pastorello et al., 2020). Data variable 'GPP_DT_VUT_MEAN' serves as the mean observed GPP, while the difference between 'GPP_DT_VUT_05' and 'GPP_DT_VUT_95' represents the uncertainty in GPP observations arising from u^* filtering, which constitutes the largest uncertainty in carbon budgets at seasonal timescales. The FLUXNET2015 dataset includes LAI and biomass measurement data for the site US-Ne2, which can indirectly or directly validate intermediate processes of a crop model, such as respiration, biomass allocation, and leaf growth. For the site IN-Hyd, which is not included in the FLUXNET2015 dataset, eddy covariance data are processed with EddyPro post-processing software (version 7.0.8, LI-COR, USA), then with the R package *REddyProc* to obtain the nighttime-partitioned GPP (Wutzler et al., 2018). The uncertainty of GPP in the site IN-Hyd (~30%) is higher than that of the site US-Ne2 (~15%) as only four months of data during maize growing season is available for analysis.

3.2 Field experiments with crop growth under elevated CO_2 or O_3 concentrations, or in combination

Elevated CO_2 and ozone exposure experiments used for the calibration and evaluation of TEMIR are listed in Table 2. All experiments were conducted in the field. Exposure of crops to elevated CO_2 and ozone concentrations was achieved with either open top chambers or FACE facilities.

https://doi.org/10.5194/egusphere-2026-5958
Preprint. Discussion started: 3 November 2026
© Author(s) 2026. CC BY 4.0 License.

Three sets of elevated CO_2 exposure experiments were selected for this study: Manderscheid et al. (2014) conducted elevated CO_2 exposure experiments for maize at 550 ppm with FACE for two growing seasons; Singh et al. (2023) conducted one growing season of elevated CO_2 exposure experiments at 700 ppm in conjunction with different ozone concentrations for maize with open-top chambers; the SoyFACE project conducted elevated CO_2 exposure experiments at 550 ppm for soybean in year 2001, 2002, and 2004 to 2006. All of the SoyFACE experiments except the one in year 2001 were also conducted with exposure to elevated ozone.

Four sets of elevated ozone exposure experiments were selected for this study: Peng et al. (2020) conducted elevated ozone exposure experiments for maize at five concentration levels ranging from 20–100 ppb (10-h mean concentration) in open-top chambers; Singh et al. (2023) conducted ozone exposure experiments at three concentration levels ranging from 0–65 ppb in conjunction with the elevated CO_2 experiments for maize; and two sets of ozone exposure experiments conducted at the SoyFACE facility. The first set of SoyFACE experiments was a set of factorial exposure experiments at two ozone levels (ambient and 125% of ambient) and two CO_2 levels (ambient and 550 ppm) in year 2004 to 2006. The second set of SoyFACE experiments were conducted at seven levels ranging from ambient (~ 35 ppb) to 200 ppb in years 2009 and 2010. In every set of selected ozone exposure experiments, measurements of the saturated photosynthetic rate and stomatal conductance were conducted at least twice during a growing season for the calibration of model parameters in the Lombardozzi scheme. Selected exposure experiments are from different major crop plantation regions, such that derived parameters are representative for evaluation at regional and global scales of ozone-induced yield loss. In addition, ozone exposure experiments should be conducted in a wide range of ozone concentrations so that derived parameters can cover occasional extreme air pollution events with ozone concentrations exceeding 150 ppb.

Table 2. Observational data used for calibration and evaluation of TEMIR v2.0 to simulate maize and soybean growth under elevated CO_2 and O_3 concentrations. In the column 'O_3 levels' are the field experiment labels used in their corresponding references, the parentheses include the new labels used in this study, followed by the 10-h mean O_3 concentrations during the O_3 fumigation period.

Site (year)	Crop	CO_2 levels	O_3 levels	Reference
SoyFACE (2001–2002)	Soybean	Ambient (aCO_2) and elevated CO_2 (eCO_2: 550 ppm)	/	e.g., Bernacchi et al. (2005) Bernacchi et al. (2006) Dermody et al. (2006)
SoyFACE (2004–2006)		aCO_2 and eCO_2 (550 ppm)	Ambient (aO_3; ~50 ppb) Elevated (eO_3; ~70 ppb)	
SoyFACE (2009–2010)		aCO_2	9 levels, between 35 and 200 ppb	Betzelberger et al. (2012)
Manderscheid (2007–2008)	Maize	aCO_2 and eCO_2 (550 ppm)	/	Manderscheid et al. (2014)
Singh (2013-2014)	Maize	aCO_2 and eCO_2 (700 ppm)	Filtered air (fO_3; ~5 ppb) Ambient (aO_3; ~50 ppb) Elevated (eO_3; ~65 ppb)	Singh et al. (2023)

https://doi.org/10.5194/egusphere-2026-5958
Preprint. Discussion started: 3 November 2026
© Author(s) 2026. CC BY 4.0 License.

Peng (2018)	Maize	aCO_2	CF (fO_3; ~20 ppb) NF (aO_3; ~40 ppb) NF40 (eO_3-lv1; ~65 ppb) NF60 (eO_3-lv2; ~85 ppb) NF80 (eO_3-lv3; ~100 ppb)	Peng et al. (2020)

4 Model simulations and data analysis

Simulations for flux tower sites US-Ne2 and IN-Hyd, as well as CO_2 or ozone exposure experiments were primarily driven with meteorological and land surface measurements at the sites. Input variables that are not available from measurements at the site are obtained from hourly MERRA-2 meteorological inputs at a 0.625° longitude × 0.5° latitude spatial resolution. The complete list of necessary variables to drive the model could be found in Table S5 in Tai et al. (2024). The model CO_2 concentration of a simulation was a constant and was adjusted for growing season years or elevated CO_2 exposure experiments. Hourly ozone concentration inputs for ozone exposure experiments of SoyFACE were obtained from Aspray et al. (2023), whereas in other ozone exposure experiments hourly ozone concentration inputs were derived from long-term (monthly or whole growing season) 24-h and 10-h mean concentrations reported at those sites.

Water stress is explicitly simulated in TEMIR v2.0 but can be turned off for irrigated crop simulations. In this study all selected sites were well irrigated and it is assumed that all crops do not experience any water stress ($\beta_t = 1$, Equation 3).

The nitrogen module of the crop model is currently in development and crops are simulated without experiencing nitrogen stress. Crops were well fertilized in all sites selected for this study, and therefore it can be assumed that all crops do not experience nitrogen stress in the simulations.

4.1 Simulations of crops at flux tower sites US-Ne2 and IN-Hyd

Two sets of simulations were conducted for the growing seasons of the flux tower sites US-Ne2 and IN-Hyd. The first set of simulations, labeled as *Ne2-constrained* and *Hyd-constrained*, were for the evaluation of the performance in simulating plant carbon budgets, without the coupling of LAI and GPP, by constraining modeled LAI with observations. Processes that change plant carbon budget include photosynthesis, respiration, biomass allocation, and senescence. Constraining modeled LAI with observations prevents any bias from the modeled GPP from propagating to the calculation of leaf growth, which can subsequently feed back to the calculation of canopy-level GPP. In the second set of simulations, labeled as *Ne2-freeLAI* and *Hyd-freeLAI*, LAI was a free variable and was simulated normally based on crop phenology (Equations 15 and 24). Phenology of crops was constrained in both sets of simulations, which was achieved by prescribing the GDD requirements of different growing stages.

The performance of TEMIR in simulating flux tower sites is based on absolute agreement with the observed GPP and biomass. Model agreements in both aboveground biomass and GPP hint at the performance in simulating crop respiration. To

https://doi.org/10.5194/egusphere-2026-5958
Preprint. Discussion started: 3 November 2026
© Author(s) 2026. CC BY 4.0 License.

quantitatively evaluate the performance of GPP simulations, statistical metrics presented in Wu et al. (2016) and Tai et al. (2024) are used (Table 3).

Table 3. Statistical metrics used to evaluate the performance of TEMIR to simulate GPP.

Metrics	Equation	Range
Coefficient of determination (R^2)	$R^2 = 1 - \frac{\sum_i (M_i - O_i)^2}{\sum_i (M_i - \bar{O})^2}$	0 to 1
Normalized mean error (NME)	$\mathrm{NME} = \frac{\sum_i \lvert M_i - O_i \rvert}{\bar{O}}$	-∞ to +∞
Normalized mean bias (NMB)	$\mathrm{NMB} = \frac{\sum_i (M_i - O_i)}{\bar{O}}$	-∞ to +∞
Index of agreement (IOA)	$\mathrm{IOA} = 1 - \frac{\sum_i (M_i - O_i)^2}{\sum_i (\lvert M_i - \bar{O} \rvert + \lvert O_i - \bar{O} \rvert)^2}$	0 to 1

4.2 Simulations of crops at CO_2 and O_3 exposure experiments

The performance of TEMIR in simulating exposure experiments is evaluated based on the agreement in the relative changes in biomass (total, aboveground, and grain) and LAI when crops are exposed to elevated concentrations of CO_2 or ozone, compared to those grown under ambient conditions. One set of simulations were conducted for the CO_2 exposure experiments (including co-exposure experiments with ozone) with LAI as a free variable with prescribed phenology, similar to the settings of *Ne2-freeLAI* and *Hyd-freeLAI*. Multiple sets of simulations were conducted for ozone exposure experiments, including those with co-exposure to elevated CO_2 concentrations. Six sets of simulations were run for soybean, which included one with ozone damage turned off (*O_3_off*), one using the default parameters of Lombardozzi scheme (*Lom_Def*; Table 1), one using the damage parameters calibrated based on Sitch scheme (*Sitch_Leung*; Leung et al., 2020), and three using damage parameters with uncertainties calibrated based on Lombardozzi scheme (*Lom_Cali*; Table 1).

For maize, a set of simulations with ozone damage turned off (*O_3_off)* and another set of simulations with the default parameters of Lombardozzi (*Lom_Def*; Table 1) were also conducted. Sensitivity simulations were conducted with $a_{\mathrm{Lombardozzi_An}}$ values calibrated to relative biomass loss observations, in addition to the intended $a_{\mathrm{Lombardozzi_An}}$ value that was calibrated to observed relative loss of A_{sat} (Peng: −0.085 m^2 $mmol^{-1}$ O_3; Singh: −0.124 m^2 $mmol^{-1}$ O_3; Fig. S2). Table 4 summarizes all the simulation sets for the flux tower sites and CO_2 and ozone exposure experiments. In some experiments the sowing density was not mentioned and biomass was reported on a per-plant basis. Simulations of these experiments assumed a typical planting density of 8 m^{-2} for maize and 35 m^{-2} for soybean, and the observed biomass was scaled accordingly for model evaluation.

https://doi.org/10.5194/egusphere-2026-5958
Preprint. Discussion started: 3 November 2026
© Author(s) 2026. CC BY 4.0 License.

Table 4. Simulation sets for the evaluation of crop growth at flux tower sites and exposure experiments.

Case name	LAI	CO_2	Ozone damage scheme
Flux tower sites US-Ne2 and IN-Hyd			
Ne2-constrained *Hyd-constrained*	Prescribed	Ambient, adjusted by growing season year	Damage turned off
Ne2-freeLAI *Hyd-freeLAI*	Variable		
CO_2 exposure experiments (Manderscheid, SoyFACE, and Singh)			
/ (not needed)	Variable	Depends on experiments (Ambient or elevated)	Damage turned off (Manderscheid) Lombardozzi, calibrated to A_{sat} (SoyFACE, Singh)
Soybean O_3 exposure experiments (SoyFACE)			
O_3_off	Variable	Ambient (2009 and 2010) Depending on experiments (2002, 2004 to 2006)	Damage turned off
Lom_Def			Lombardozzi, default parameters
Sitch_Leung			Sitch, parameters calibrated by Leung et al. (2020)
Lom_Cali			Lombardozzi, calibrated to A_{sat} $a_{Lombardozzi}$ = −0.022±0.006 m^2 $mmol^{-1}$ O_3 (Fig. S1)
Maize O_3 exposure experiments (Peng and Singh)			
O_3_off	Variable	Depending on experiments	Damage turned off
Lom_Def		Depending on experiments	Lombardozzi, default parameters
LomCali_Peng (only for Peng)		Ambient	Lombardozzi, calibrated to A_{sat}, AGB, and yield $a_{Lombardozzi}$ range from −0.01 to −0.085 m^2 $mmol^{-1}$ O_3
LomCali_Singh (only for Singh)		Depending on experiments	Lombardozzi, calibrated to A_{sat}, total BM, and yield $a_{Lombardozzi}$ range from −0.03 to −0.124 m^2 $mmol^{-1}$ O_3

5 Results and discussion

5.1 Descriptions and the simulation results of flux tower site US-Ne2 and IN-Hyd

Figure 1 compares the observed and simulated daily GPP when LAI is constrained to observations in *Ne2-constrained*. The model overestimates GPP for maize and underestimates GPP for soybean in general. Values of NMB and NME for maize are +26.6% and 30.3%, respectively, whereas those for soybean are −8.4% and 17.4%. R^2 and IOA values for maize GPP reach 0.816 and 0.893, whereas those for soybean are 0.773 and 0.887. Positive bias in maize GPP occurs at the late growing stage, which can be partially explained by the lack of parameterization of the decline in photosynthetic capacity on leaf-level when

https://doi.org/10.5194/egusphere-2026-5958
Preprint. Discussion started: 3 November 2026
© Author(s) 2026. CC BY 4.0 License.

crops senesce in the model. Negative bias in soybean occurs during the middle growing stage, which could be related to the values of biochemical parameters that are not calibrated to the US-Ne2 site.

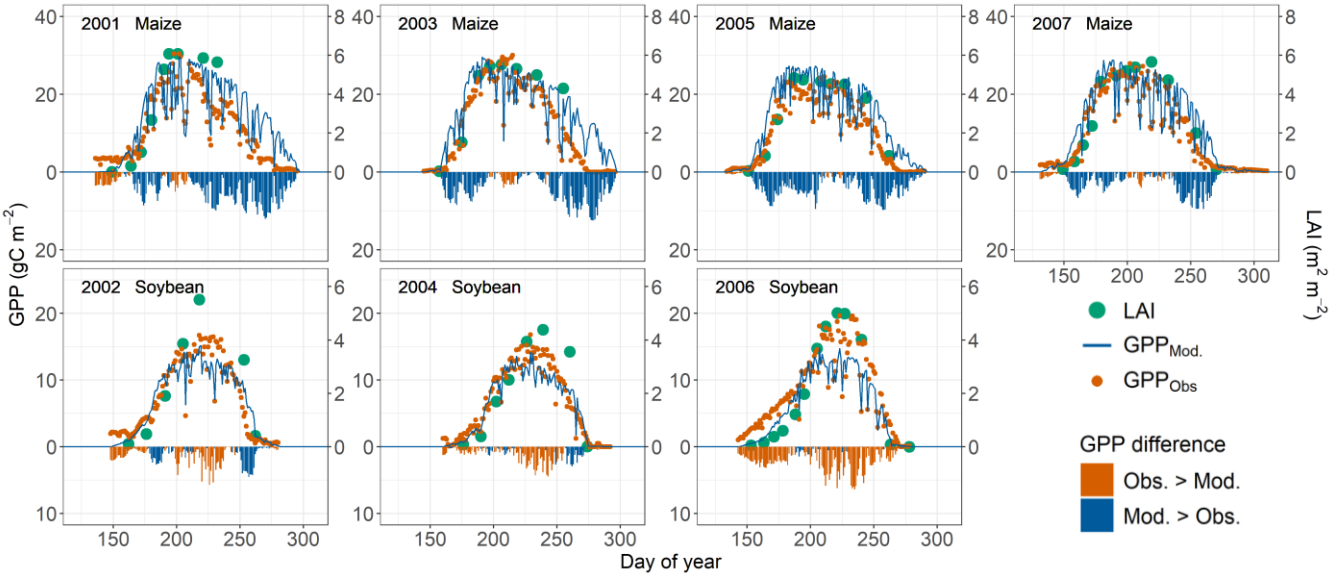


Figure 1. Observed and modeled daily mean GPP of the simulation case *Ne2-constrained*, as well as the difference of the two values.

Figure 2 illustrates the cumulative bias in GPP and the difference between observed and modeled aboveground biomass. The cumulative bias in maize GPP features an increase that is larger than the uncertainty of the observed GPP during the early and late growing season. For maize, the model overestimates the growing season GPP by 300–500 gC m^{-2}, which is larger than the upper bound uncertainty of the observations of 4–130 gC m^{-2}. The excess modeled GPP leads to overestimation of modeled aboveground biomass of 125–250 gC m^{-2} during the late growing stage. Simulated growing season GPP and aboveground biomass for soybean agree with observed values within uncertainties in year 2002 and 2004, while in year 2006 the modeled GPP underestimates the observed value by 80–320 gC m^{-2}.

https://doi.org/10.5194/egusphere-2026-5958
Preprint. Discussion started: 3 November 2026
© Author(s) 2026. CC BY 4.0 License.

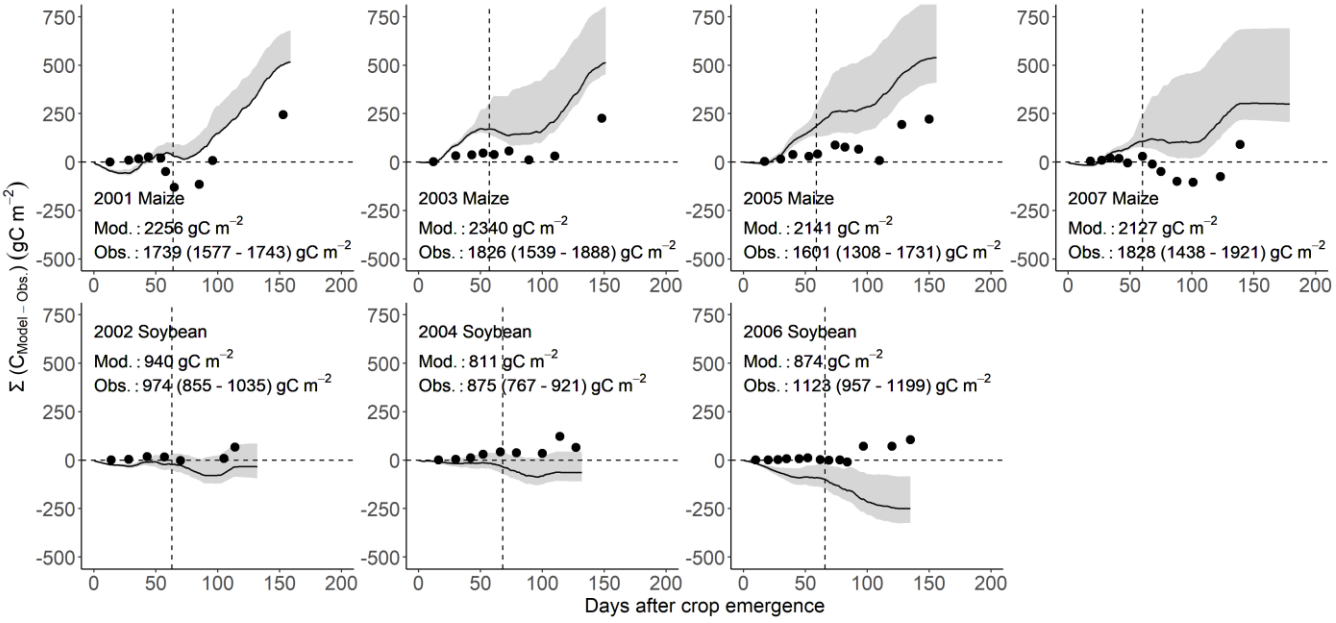


Figure 2. Difference in the modeled and observed plant carbon budgets (dots: above-ground biomass; lines: cumulative GPP) of the growing seasons of the US-Ne2 site. Shaded area represents the range of the difference in cumulative GPP calculated with FLUXNET GPP products GPP_DT_VUT_05 and GPP_DT_VUT_95. Vertical dashed lines indicate the estimated start of the crop reproductive stage. Annotated numbers represent the model and observed cumulative GPP at the end of a growing season.

Time series of the modeled and observed aboveground biomass and crop yield are shown in Figure 3. Modeled above ground biomass for both maize and soybean agree with the observed values before the late growing stage, which indirectly validates the calculation of plant respiration, presuming that the simulated root biomass has reasonable agreement with root biomass in the field. Both the observed maize and soybean aboveground biomasses increase steadily in the middle growing season and then decline during the late growing stage. The decline in the biomass growth is attributed to both reducing available GPP and direct loss of biomass from leaf senescence. In the maize model, the surplus GPP at the late growing stage is mostly allocated to the reproductive part (i.e., grain), which is reflected by the ~80% or ~ +400 gC m^{-2} positive bias in the simulated grain biomass and an unusually high modeled harvest index of around 0.8. Among the surplus grain biomass of 350–400 gC m^{-2}, the surplus aboveground biomass contributes around 250 gC m^{-2} (Figure 2) while the rest is attributed to carbon retranslocation (Equation 22) and the uncertainty in phenology and allocation coefficients (Equation 19).

https://doi.org/10.5194/egusphere-2026-5958
Preprint. Discussion started: 3 November 2026
© Author(s) 2026. CC BY 4.0 License.

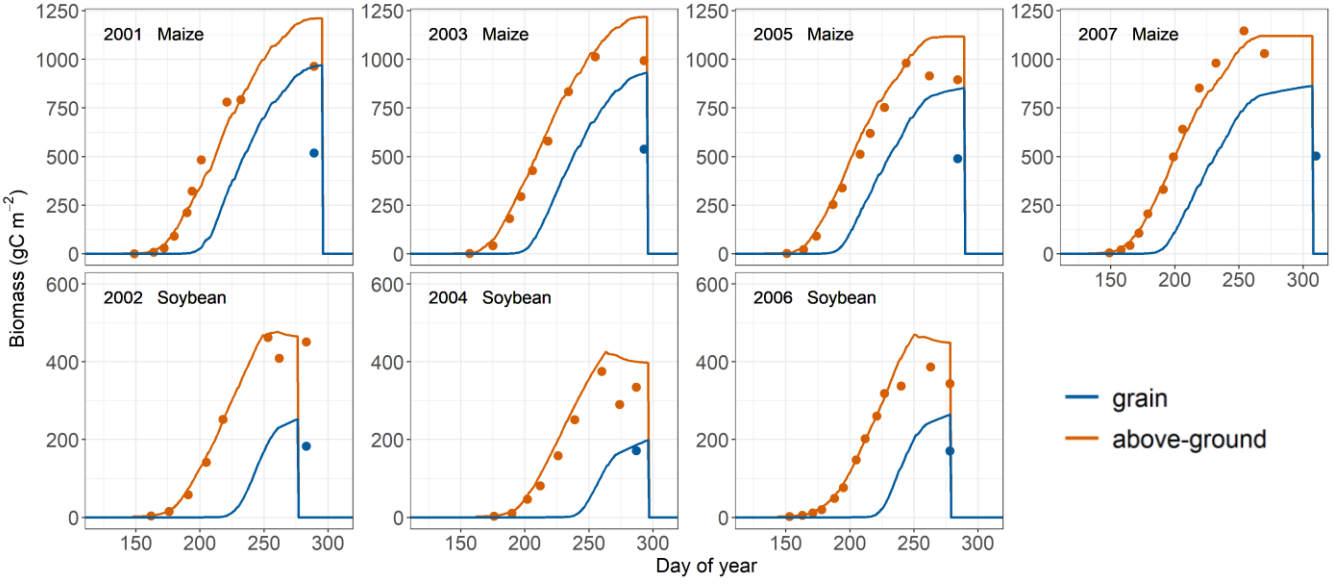


Figure 3. Observed (dots) and modeled (lines) above-ground and grain biomass in the simulation case *Ne2-constrained*.

Simulations of LAI and crop height are shown in Figure 4. In *Ne2-freeLAI*, the peak LAI reaches 8 m^2 m^{-2} for soybean, which is 3 m^2 m^{-2} higher than observations. In *Ne2-constrained* where LAI is constrained to observed values, the equivalent LAI derived from leaf carbon (Equation 24) has satisfactory agreement with observations. The high modeled peak LAI in *Ne2-freeLAI* can be explained by the high initial LAI value at emergence of ~0.07, higher than the measurement values of 0.02–0.06 recorded one to two weeks after emergence. In addition, the positive feedback of GPP-LAI-photosynthesis can lead to excessive canopy growth. Crop height modeled in *Ne2-constrained* agrees with the observed values during the early- to mid-growing season, and it is slightly underestimated at the late growing stages. The underestimated crop height and thereby stem biomass complement the high bias in modeled grain biomass, indicating the allocation coefficients contribute to the error in the simulation of crop yield.

https://doi.org/10.5194/egusphere-2026-5958
Preprint. Discussion started: 3 November 2026
© Author(s) 2026. CC BY 4.0 License.

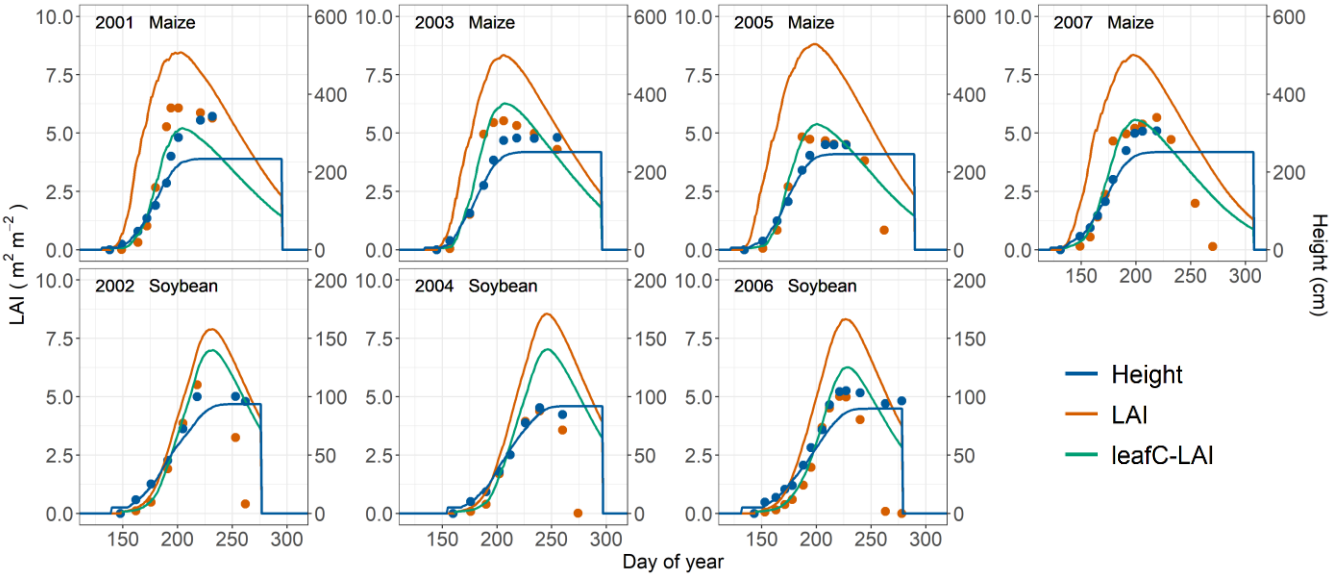


Figure 4. Observed (dots) and modeled (lines) LAI in the simulation case *Ne2-freeLAI* modeled with the recorded planting density, as well as the crop height and the LAI derived from leaf carbon pool (Equation 24) in the simulation case *Ne2-constrained.*

Figure 5 summarizes the simulation results of the tropical irrigated maize flux tower site IN-Hyd. Compared to maize grown at the site US-Ne2, maize at IN-Hyd has a shorter growing season of ~100 days than that at US-Ne2 (~170 days). A shorter growing season results in a low observed growing season GPP of about 800 gC m^{-2}, a low maximum growing season LAI of 3.5 m^2 m^{-2}, as well as a low measured aboveground biomass of around 600 gC m^{-2}. In *Hyd-constrained* where LAI is prescribed with observations, values of NMB, NME, R^2, and IOA of the simulated daily averaged GPP are +50.6%, 56.0%, 0.307, and 0.586, respectively. These statistical metrics suggest that the performance of the simulation of tropical maize GPP is inferior to that of the simulation of maize GPP at the site US-Ne2. The general high bias in the simulated daily average GPP accumulates and propagates to the modeled growing season GPP, for which a positive bias of ~50% or 400 gC m^{-2} is obtained (Fig. 5a). Despite the high bias in the simulated GPP, the model aboveground biomass is within 15% or 100 gC m^{-2} of the observed values during the early- and mid-growing season (Fig. 5b). Similar to the simulations of US-Ne2, modeled grain yield overestimates the observed value by ~80% (~200 gC m^{-2}) (Fig. 5c). In the simulation of crop height and LAI of the site IN-Hyd (Fig. 5d), model performance is inferior to that of US-Ne2, as both of the allometric and biomass allocation parameters are mainly derived from temperate maize observation data from US-Ne2 and other FLUXNET2015 or AmeriFlux sites. Tropical maize is expected to have different allometric relationships and phenology than that of temperate maize, such as the preferential allocation toward leaf biomass as well as the delayed timing of leaf senescence (Infante et al., 2018). Nevertheless, TEMIR can capture the lower maximum LAI as observed in the field compared to the observed maximum LAI at the temperate US-Ne2 site.

https://doi.org/10.5194/egusphere-2026-5958
Preprint. Discussion started: 3 November 2026
© Author(s) 2026. CC BY 4.0 License.

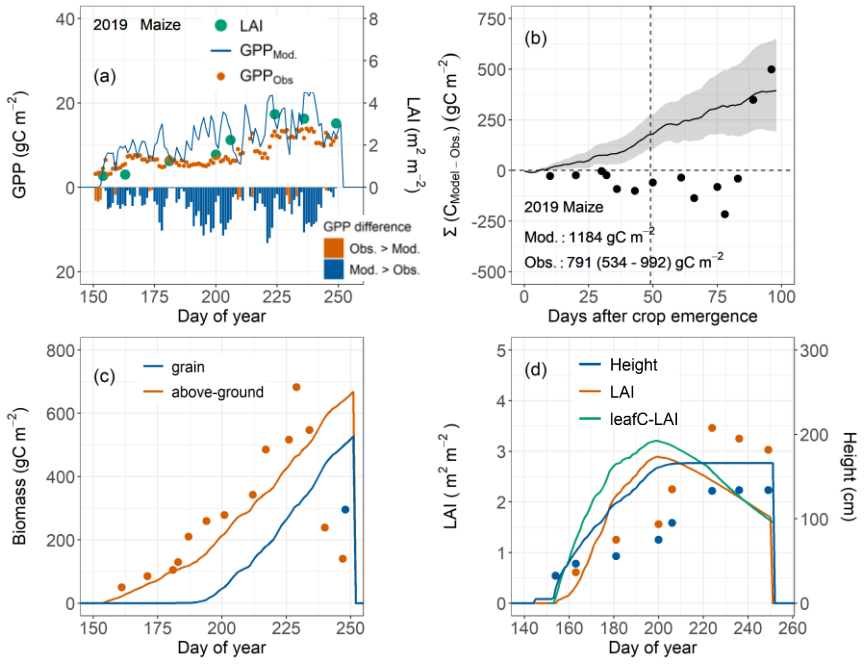


Figure 5. Observed and modeled maize growth at the Indian tropical irrigated site in year 2019. Plots follow Figure 1 to Figure 4, which include (a) comparison of the daily GPP; (b) comparison of the cumulative GPP and biomass difference, where the uncertainty of the GPP measurement is 30%; (c) comparison of the above-ground biomass and harvested yield; and (d) modeled crop height, LAI derived from leaf carbon in simulation case *Hyd-constrained*, as well as the simulated LAI in case *Hyd-freeLAI*.

The plant carbon budgets of eddy covariance sites can be examined by the NPP:GPP ratio and harvest index (HI). The NPP:GPP ratio indicates the amount of assimilated carbon lost from respiration. Typically, the NPP:GPP ratio reduces with increasing temperature as respiration loss increases with temperature, while photosynthetic rate plateaus and eventually declines when temperature reaches ~40 °C (Rotundo et al., 2019; Luo et al., 2025). Using above-ground biomass measurements as a proxy for NPP, NPP:GPP ratios for maize at sites US-Ne2 and IN-Hyd are estimated to be 55–61% and ~75%, respectively. The NPP:GPP ratio of the site US-Ne2 is similar to that from other eddy covariance (EC) sites with maize plantations in temperate regions (44–68%, Table S3), while the NPP:GPP ratio of the site IN-Hyd is ~15 percentage points higher than values reported where maize was grown under comparatively cooler conditions. The reason for this unusually high NPP:GPP ratio at IN-Hyd remained uncertain; however, a systematic negative bias in GPP measurements can reconcile the disparity between modeled and measured GPP. EC-derived GPP is calculated through the partitioning of measured net ecosystem exchange (NEE) flux, and factors such as energy balance non-closure, partitioning method, low turbulence conditions, etc., can introduce systematic biases. In an EC measurement campaign in a southern Indian tropical rice system that has a similar climate to site IN-Hyd (Oo et al., 2023), the ratio between the harvested biomass (grain and straw) and the EC-derived GPP (i.e., ~NPP:GPP) ranged from 57–98% (assuming a 14% moisture content in harvested). The unusually high NPP:GPP obtained from EC-crop systems in tropical climates might indicate systematic underestimation of GPP. Modeled NPP:GPP ratios of maize for both

https://doi.org/10.5194/egusphere-2026-5958
Preprint. Discussion started: 3 November 2026
© Author(s) 2026. CC BY 4.0 License.

US-Ne2 and IN-Hyd range from 0.52–0.55, consistent with the observed NPP:GPP ratio of temperate maize. However, the model does not simulate a lower NPP:GPP ratio at IN-Hyd, where the average growing season temperature is 8 °C higher than that of US-Ne2.

Observed maize harvest indices from sites US-Ne2 and IN-Hyd range from 0.43–0.54, which agree well with values (0.50–0.57) determined from other studies (Table S3). Modeled maize harvest indexes range from 0.76–0.80 for both sites US-Ne2 and IN-Hyd, which are reflected by the high bias in the simulated maize yield. One way to resolve the high bias in the simulated crop yield in TEMIR is to use a constant harvest index of 0.5 and modeled aboveground biomass to derive grain yield. With the uncertainty of the observed harvest indices (20%, or 0.5 ± 0.1) and the relatively low bias in modeled aboveground biomass (25%, Figure 3), grain yield derived from aboveground biomass and HI would have a combined uncertainty of ~32%, which is much smaller than the bias of the grain yield calculated through NPP allocation and retranslocation (Equations 19 and 22).

5.2 Simulations of crop exposure experiments

5.2.1 Effects of elevated CO_2 on biomass and LAI

Figure 6 compares the modeled and observed relative biomass under exposure to elevated CO_2 concentrations, relative to that under exposure to ambient CO_2 concentrations. No significant change in the aboveground biomass, crop yield, and LAI are observed for maize exposed to 550 ppm of CO_2 concentration from the Manderscheid dataset, whereas a 5–15% increase in biomass and a small increase in LAI of less than 0.25 m^2 m^{-2} at 700 ppm CO_2 are observed from the experiments conducted by Singh et al. (2023) (Figure 7). TEMIR reproduces the insensitivity of maize growth at 550 ppm CO_2 relative to the ambient CO_2 levels, but overestimates relative total biomass and relative crop yield by 25 percentage points and 5 percentage points, respectively, for maize growth at 700 ppm CO_2. The high bias in simulated relative crop yield is caused by overestimation of peak LAI, which then propagates to the modeled plant carbon intake during the crop reproductive stage. The bias in the simulated relative total biomass is much less than that for the relative crop yield, as measurements of total biomass were taken during the mid-growing season (mid-February), when differences in modeled LAI among various ozone and CO_2 treatments were still small.

Soybean growth shows a more pronounced positive response to elevated CO_2 concentrations at 550 ppm than that of maize, as expected for a C_3 plant. Observed relative aboveground biomass and crop yield increase by 6–29% and 7–24%, respectively; observed LAI increases by ~0.4 m^2 m^{-2} at mid-growing season under the exposure to elevated CO_2. TEMIR reproduces the CO_2 fertilization effect on soybean growth, but the impacts are generally exaggerated. Modeled increases in relative biomass under the exposure to elevated CO_2 range from 20–30%, which can be explained by the high bias in peak LAI of 2 m^2 m^{-2}. Again, the high bias in LAI propagates to the calculation of plant carbon uptake.

https://doi.org/10.5194/egusphere-2026-5958
Preprint. Discussion started: 3 November 2026
© Author(s) 2026. CC BY 4.0 License.

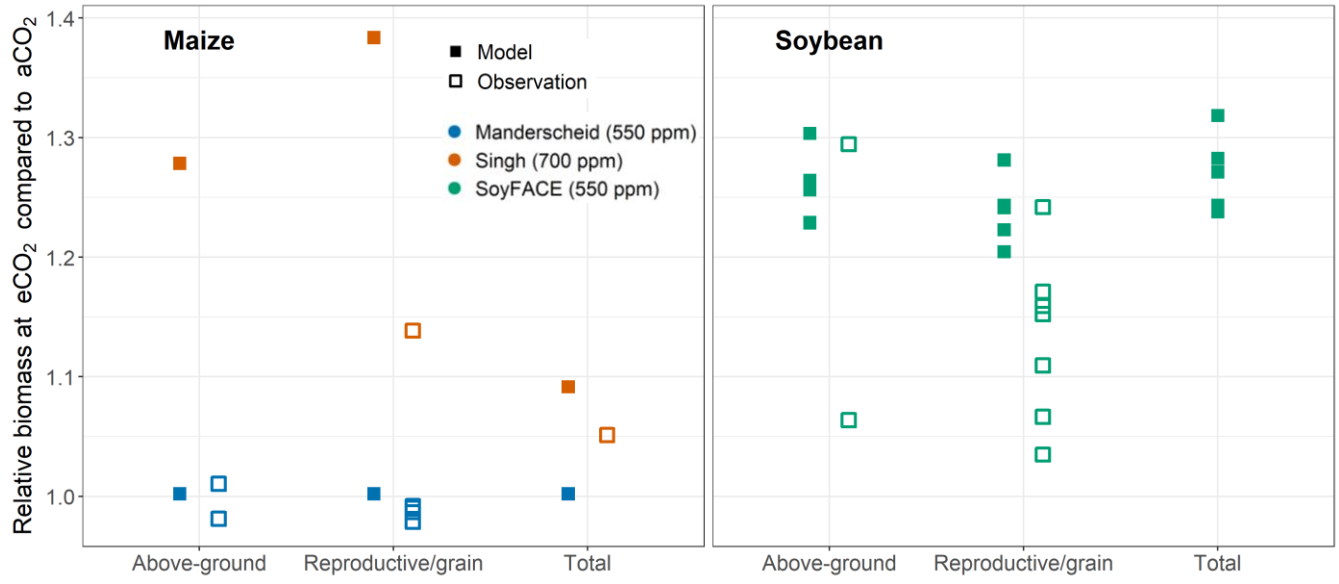


Figure 6. Modeled and observed relative biomass for crops exposed to elevated CO_2 concentrations relative to that in ambient CO_2 concentrations. Each model and observation data point represents one growing season and model data points of the Manderscheid dataset are overlapped. All biomass measurements were taken near the end of a growing season, except for the total biomass of the growing season in the Singh dataset that was taken during the mid-growing season.

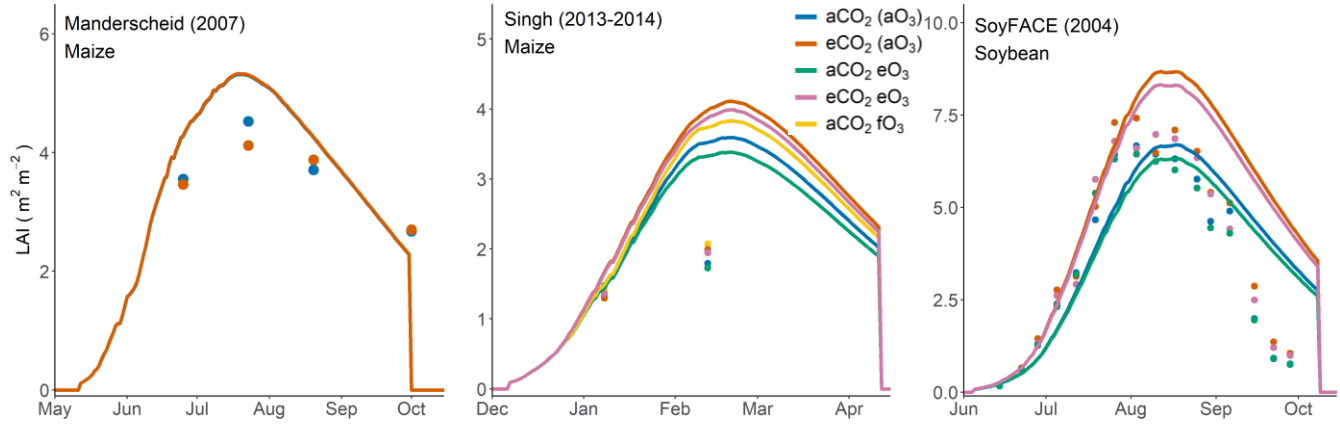


Figure 7. Selected years of modeled and observed LAI for crops grown in different conditions in CO_2 exposure experiments.

https://doi.org/10.5194/egusphere-2026-5958
Preprint. Discussion started: 3 November 2026
© Author(s) 2026. CC BY 4.0 License.

5.2.2 Effects of elevated O_3 on biomass and LAI in soybean

Figure 8 compares the observed and modeled relative biomass at different ozone levels for soybean. For the ozone exposure experiments in years 2009 and 2010 (Figure 8a), using the parameters calibrated for the Lombardozzi scheme (case *Lom_Cali*) has the best performance in predicting relative yield loss over the default Lombardozzi parameters (*Lom_Def*) and calibrated Sitch parameters (*Sitch_Leung*). The mean error in simulating relative yield loss in case *Lom_Cali* is 0.047, while those in cases *Lom_Def* and *Sitch_Leung* range from 0.25–0.30. In *Lom_Def*, a high positive relative yield of +35% is obtained when ozone damage is turned off, compared to the reference simulation with ambient ozone concentrations. Modeled relative yield loss is very insensitive to further increase in ozone exposure, which can be explained by the values of ozone damage parameters $b_{\text{Lombardozzi_An}}$ and $a_{\text{Lombardozzi_An}}$ in the default Lombardozzi scheme (Table 1). In simulation case *Sitch_Leung*, results are characterized by an insensitive yield loss response when the target ozone level is below 70 ppb, followed by a yield loss response that is comparable to the observed values at target ozone concentrations between 70 ppb and 200 ppb (AOT40 > 20 ppm h). The lack of yield loss response at lower ozone levels is associated with the high F_{crit} value of 15 nmol O_3 m^{-2} s^{-1} calibrated in Leung et al. (2020), much higher than the F_{crit} value of 9.6 nmol O_3 m^{-2} s^{-1} derived for the Chinese soybean (Zhang et al., 2017), and values of 3–6 nmol O_3 m^{-2} s^{-1} for generic crops for large-scale modeling assessment (CLRTAP, 2023). In *Lom_Cali*, modeled crop yield without ozone damage is ~5% higher than that with damage under ambient ozone levels, consistent with the defined critical level of ozone damage. Figure 9 compares observed and modeled LAI at different ozone concentrations. At exposure experiments that have the highest target ozone concentrations, observed peak LAI reduces by ~2 m^2 m^{-2} relative to the reference ambient experiment. TEMIR generally reproduces the reduction of vegetation-stage LAI under ozone exposure well in both *Lom_Cali* and *Sitch_Leung*.

Figure 8b is a similar comparison of modeled and observed relative biomass loss for the exposure experiments in years 2002, 2004–2006. Target ozone concentrations of elevated ozone experiments in these years are lower (70–100 ppb) compared to the highest ozone levels (200 ppb) in the experiments in years 2009 and 2010. Therefore, a lower maximum ozone-induced relative biomass loss is observed for experiments in years 2002, and 2004–2006 than that in years 2009 and 2010. At ambient CO_2 levels, the observed reduction in crop yield under exposure to elevated ozone ranges from 3.5–18.4%, after excluding an outlier growing season where a 10% increase in crop yield under elevated ozone is observed. In simulation case *Sitch_Leung*, the relative reduction of crop yield ranges from 0–2.5%, while in *Lom_Cali* the modeled relative reduction of crop yield ranges from 10.0–16.7%. At elevated CO_2 levels, the observed relative yield loss under elevated O_3 concentration ranges from 1.4–10.1 %, suggesting an elevated CO_2 concentration of 550 ppm alleviates ozone-induced damage at 370 ppm CO_2 by 20–60%. The modeled relative ozone-induced yield loss under elevated CO_2 in *Sitch_Leung* is zero, as ozone damage is already insignificant under ambient CO_2 levels. In *Lom_Cali*, the modeled relative yield loss ranges from 7.5–10.8%, which is slightly higher than the observed values. Overall, model performance in simulating ozone-induced yield loss in case *Lom_Cali* is superior to that in case *Sitch_Leung*.

https://doi.org/10.5194/egusphere-2026-5958
Preprint. Discussion started: 3 November 2026
© Author(s) 2026. CC BY 4.0 License.

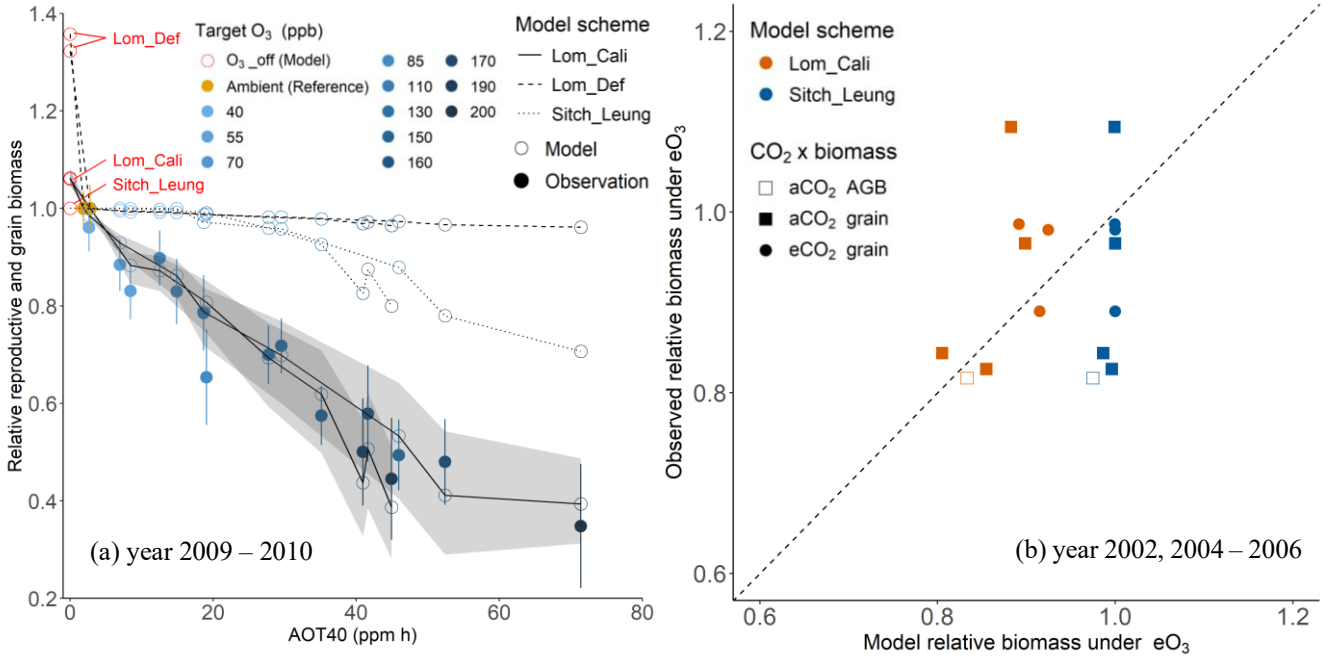
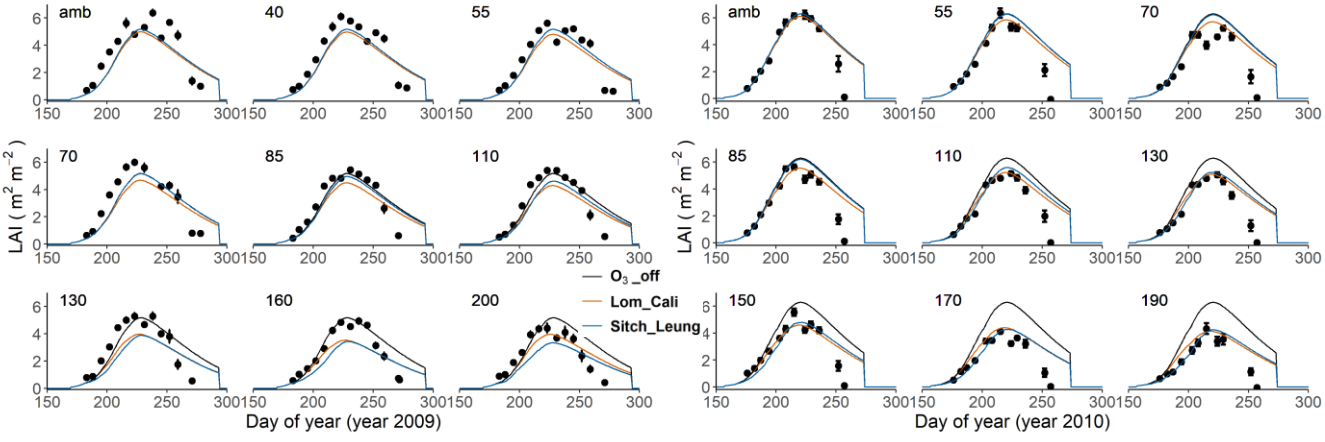


Figure 8. (a) Modeled and observed relative soybean yield under different O_3 concentration levels at ambient CO_2 for the SoyFACE experiments in year 2009 and 2010. Each model scheme has two lines connecting model results, which represent the two growing seasons. The error bars represent one standard error of the relative yield; the grey shaded area represents the range of the modeled relative yield loss in the sensitivity simulations with $a_{Lombardozzi} = -0.022 \pm 0.006$ m^2 mmol^{-1} O_3. (b) A comparison between the observed and modeled relative biomass (grain and above-ground) for the SoyFACE exposure experiments in year 2002, and 2004 to 2006. Biomass values of the ambient O_3 experiments (including exposure under ambient or elevated CO_2) are taken as reference.



https://doi.org/10.5194/egusphere-2026-5958
Preprint. Discussion started: 3 November 2026
© Author(s) 2026. CC BY 4.0 License.

Figure 9. Modeled (lines) and observed (points with error bars) LAI of the soybean ozone exposure experiments of SoyFACE in year 2009 and 2010. The target ozone concentration of each experiment is labeled at the top left of every subplot. The simulated LAI without ozone damage ('*O_3_off*') is added in every subplot for visualizations of the modeled ozone effect.

5.2.3 Effects of elevated O_3 on maize biomass

Figure 10 illustrates modeled and observed relative biomass under ozone exposure for maize based on the data collected by Peng et al. (2020). Relative to maize exposed to a below-ambient level of ozone concentration (f_{O3}, 20 ppb), aboveground biomass is reduced by 18±6% at ambient levels of ozone (aO_3, 40 ppb), and by 36±7% at the highest ozone level (eO_3-lv3, ~100 ppb). Relative to the experiment conducted with f_{O3}, no significant reduction in crop yield was observed at ambient ozone and the first elevated ozone level (eO_3-lv1, 60 ppb); reductions of 11±8% and 29±7% were observed for the second elevated ozone level (eO_3-lv2, 80 ppb) and the highest ozone level, respectively. The discrepancy between responses of aboveground biomass and crop yield to ozone exposure require different values of the ozone sensitivity parameter $a_{Lombardozzi_An}$ to achieve an optimal model-observation agreement. With an $a_{Lombardozzi_An}$ value of −0.085 m^2 $mmol^{-1}$ O_3, which is the sensitivity calibrated to relative A_{sat} to cumulative ozone uptake (Fig. S2), the model overestimates the reduction in relative aboveground biomass by 30 percentage points for experiments conducted under elevated ozone concentrations. The error increases to 20–60 percentage points for the simulation of relative crop yield for both ambient and elevated ozone concentration experiments. To reconcile modeled and observed relative aboveground biomass and crop yield, $a_{Lombardozzi_An}$ has to be reduced to −0.05±0.02 and −0.02±0.01 m^2 $mmol^{-1}$ O_3, respectively. Modeled relative grain biomass is more sensitive to ozone damage than modeled above-ground biomass at a given $a_{Lombardozzi_An}$ value, as the allocation of grain biomass takes place during the late growing stages when plants have already accumulated sufficient amount of ozone damage. It should be noted that if the analysis of the ozone-induced loss of relative aboveground biomass and relative crop yield takes the ambient ozone (aO_3) as the reference level, treating the aboveground biomass measurements under f_{O3} ozone level as an outlier, aboveground biomass and crop yield would have statistically similar sensitivities to cumulative ozone uptake (i.e., $a_{Lombardozzi_An}$ = −0.02±0.01 m^2 $mmol^{-1}$ O_3).

https://doi.org/10.5194/egusphere-2026-5958
Preprint. Discussion started: 3 November 2026
© Author(s) 2026. CC BY 4.0 License.

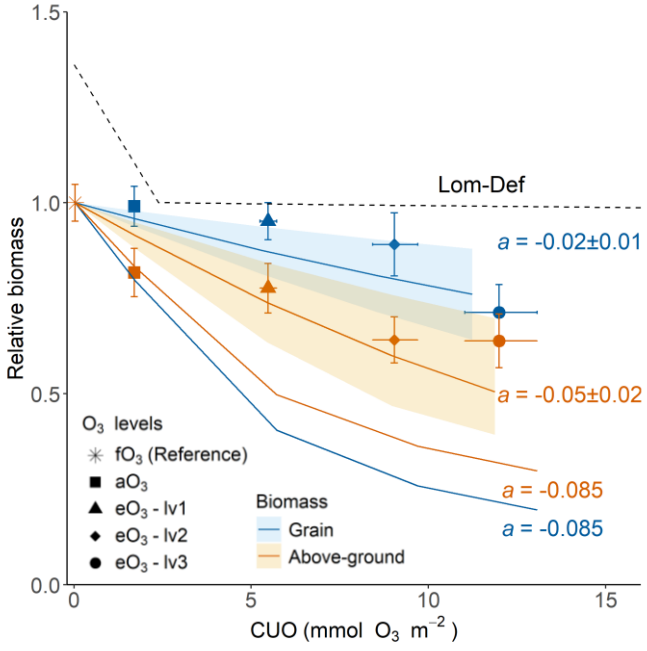
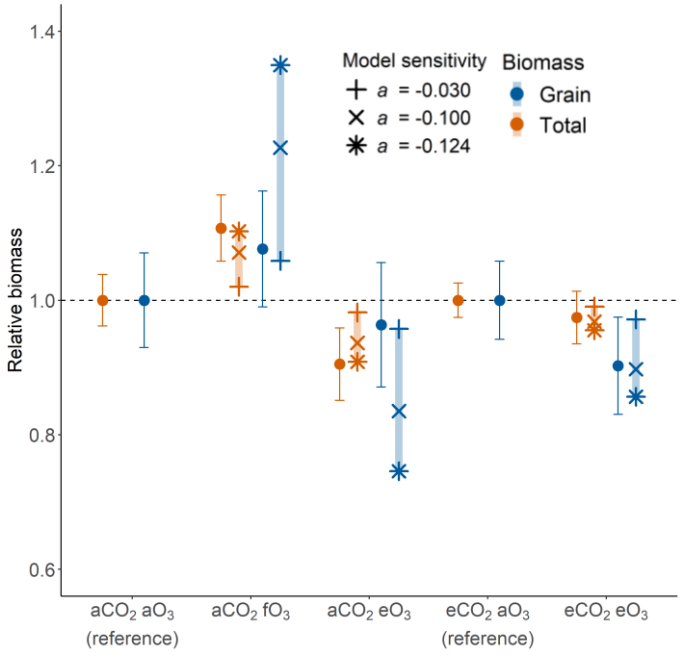


Figure 10. Observed (points and error bars) and modeled (line and shade) relative biomass under ozone exposure for the experiments conducted in Peng et al. (2020). The dashed line represents the relative biomass simulated using the default parameters of the Lombardozzi scheme. The horizontal error bar represents the range of simulated CUO at different values of the sensitivity parameter $a_{\text{Lombardozzi_gs}}$ that indirectly modify stomatal conductance and thereby CUO; the vertical error bar represents 1 standard error of the observations. The colored lines and shaded area represent the range of the modeled relative biomass at different values of $a_{\text{Lombardozzi_An}}$. The descriptions of the ozone levels can be found in Table 2.

A similar pattern, requiring a wide range of $a_{\text{Lombardozzi_An}}$ values was found to achieve good agreement in simulating relative total biomass and grain biomass under ozone exposure for the experimental data collected by Singh et al. (2023) (Figure 11). Under ambient CO_2 concentrations, observed total biomass and grain biomass under exposure to filtered air (aCO_2fO_3) are 11±5% and 8±9% higher than those exposed to ambient O_3 levels (aCO_2aO_3), respectively. On the other hand, exposure to elevated O_3 (aCO_2eO_3) leads to reductions in total biomass and grain biomass by 10±5% and 4±9%, respectively. Under elevated CO_2, exposure to the elevated O_3 (eCO_2eO_3) only reduces the observed total biomass and grain biomass by 3±4% and 10±7% relative to those in ambient ozone concentrations (eCO_2aO_3), respectively. With a value of $a_{\text{Lombardozzi_An}}$ at -0.124 m^2 $mmol^{-1}$ O_3, which is the sensitivity of the loss of relative A_{sat} to cumulative ozone uptake (Fig. S2), simulated relative total biomass is within 2 percentage points of the observed values at different ozone and CO_2 levels, while errors of the simulated relative grain biomass are about 25 percentage points at ambient CO_2 concentrations and 5 percentage points at elevated CO_2 concentrations. With value of $a_{\text{Lombardozzi_An}}$ of −0.100 m^2 $mmol^{-1}$ O_3, which is about the mean sensitivity of the loss of relative A_{sat} to cumulative ozone uptake at the two maize ozone exposure sites Peng and Singh, the error of the simulated relative crop yield at ambient CO_2 concentrations is still larger than the observed value uncertainty. To optimize the agreement between modeled and observed relative grain biomass at different levels of ozone exposure, the plant-ozone sensitivity parameter

https://doi.org/10.5194/egusphere-2026-5958
Preprint. Discussion started: 3 November 2026
© Author(s) 2026. CC BY 4.0 License.

585 $a_{Lombardozzi_An}$ has to be reduced to -0.03 m^2 $mmol^{-1}$ O_3. The analysis of the two maize sites suggests that the observed sensitivity of the reduction in relative grain yield to ozone is about one-fourth of that for relative A_{sat}. Total and aboveground biomass show diverse responses to ozone damage in the two sites, with the reduction in total biomass measured in Singh aligning with the reduction in A_{sat}, whereas the reduction in aboveground biomass measured in Peng aligns with the reduction in grain yield.



590

Figure 11. Observed (points) and modeled (plus, cross and asterisk) relative biomass under ozone exposure at two CO_2 concentrations for the experiments conducted in Singh et al. (2023). The error bars represent 1 standard error of the observed values. Three $a_{Lombardozzi}$ (in m^2 $mmol^{-1}$ O_3) values are selected for the sensitivity simulations: -0.124 is the derived sensitivity from the relationship between relative A_{sat} and CUO based on the data in Singh et al. (2023); - 0.100 is the mean sensitivity from the A_{sat}-CUO 595 **relationship of the two maize site, Singh et al. (2023) and Peng et al. (2020); -0.030 is the optimal sensitivity that yields the best agreement in the relative grain biomass.**

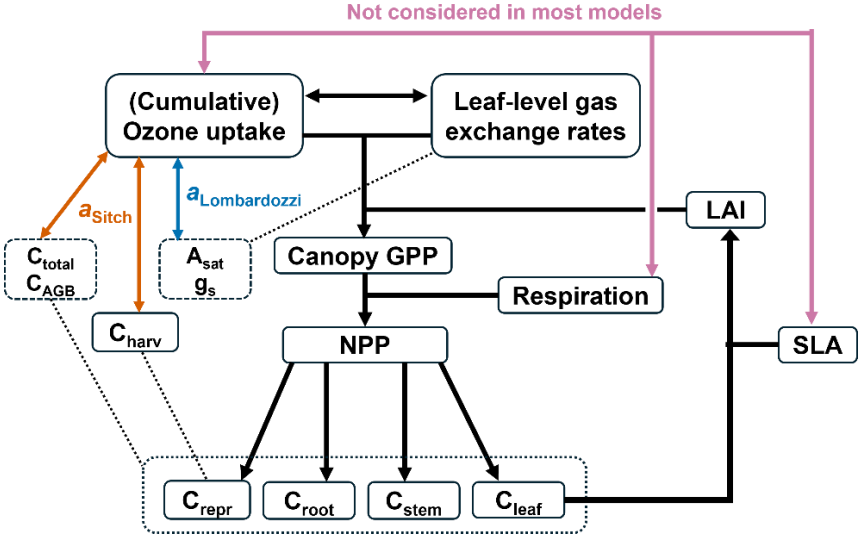
5.3 Discrepancies in sensitivities of A_{sat} and biomass to cumulative ozone uptake

The simulation results presented in Sections 5.2.2 and 5.2.3 reveal that relative reduction in soybean A_{sat} is similar to that in 600 soybean grain yield, whereas relative reduction in A_{sat} is about three to four times more sensitive to ozone than that of grain yield in maize. To explain the discrepancy in sensitivities of different variables to cumulative ozone uptake, the calculation flow of a TEMIR crop simulation is illustrated in Figure 12. On the basis of vegetation carbon budget conservation, if the reduction in total biomass due to ozone exposure is less sensitive than that of the reduction in A_{sat}, the reduction in respiration due to ozone exposure has to be more pronounced than the reduction in A_{sat} to compensate for the loss of assimilated carbon.

https://doi.org/10.5194/egusphere-2026-5958
Preprint. Discussion started: 3 November 2026
© Author(s) 2026. CC BY 4.0 License.

However, SoyFACE experiments revealed that plant respiration per mass increased for soybean (Gillespie et al., 2012), and did not significantly change for maize with increasing O_3 exposure (Li et al., 2022). To explain the lower sensitivity of the loss of aboveground biomass to O_3 than that for A_{sat} to O_3, a reduction in plant root-shoot ratio under elevated ozone exposure can offset the loss of aboveground biomass from reduced photosynthetic rate. However, meta-analyses conducted by Morgan et al. (2003) and Li et al. (2021) concluded that the change in root-shoot ratio of soybean was not significant. The Peng experimental dataset also suggested that root-shoot ratio of maize did not change significantly under elevated O_3 exposure (Peng et al., 2020).

The goal of the implementation of the Lombardozzi scheme is to simulate the effects of prolonged ozone exposure on the decoupling of global carbon and water cycles (Lombardozzi et al., 2015; Li et al., 2024). In crop simulations, the Lombardozzi scheme better reproduces the negative responses of the photosynthetic rate to chronic ozone exposure and nonresponses to acute ozone exposure, as observed in Betzelberger et al. (2012) for soybean, compared to the Sitch scheme. The similar sensitivities of the observed A_{sat} and crop yield to cumulative ozone exposure result in very good agreements in the simulated relative yield loss and reduction in LAI under ozone exposure with the TEMIR model. However, maize field experiments conducted by Peng et al. (2020) and Singh et al. (2023) suggested that there are gaps between the sensitivities of photosynthetic parameters and biomass parameters to ozone exposure. As a result, the model ozone sensitivity parameter $a_{Lombardozzi_An}$, which originally represents the reduction of the photosynthetic rate due to chronic ozone exposure, has to be reduced by 75% to reproduce the observed change in biomass and yield for maize. It is recommended that users adopt the ozone sensitivity parameter $a_{Lombardozzi_An}$ that is calibrated to relative biomass loss (i.e., −0.02 to −0.05 m^2 $mmol^{-1}$ O_3) rather than that calibrated to the relative loss of A_{sat} (~ −0.1 m^2 $mmol^{-1}$ O_3) for maize, given that the goal of simulations is to examine regional or global yield and biomass loss under chronic ozone exposure in different climate scenarios.



https://doi.org/10.5194/egusphere-2026-5958
Preprint. Discussion started: 3 November 2026
© Author(s) 2026. CC BY 4.0 License.

Figure 12. Simplified flow chart of the crop model calculation in TEMIR. Black arrows indicate the flow of variables for calculations of next step; black dashed lines indicate variables that are related to each other; colored arrows indicate variables that are used for derivation of crop-ozone sensitivities in various model studies and field studies.

5.4 Potential improvements to LAI simulation

TEMIR can simulate the positive influence on LAI from the exposure to elevated CO_2, as well as the negative influence on LAI from the exposure to elevated ozone, but the effects are generally overestimated. The current model does not take into account the impacts of changing CO_2 and O_3 concentrations on specific leaf area (SLA). SLA is usually implemented as a constant plant trait in land surface models such as CLM 4.5, or as a variable that only responds to changing phenology in crop models such as JULES-crop (Equation 25). The meta-analysis conducted by Ainsworth and Long (2005) suggests that SLA for C_3 grasses decreases by 8±4% (i.e., leaves become thicker) under elevated CO_2, while for C_4 grasses the change in SLA at elevated CO_2 is not significant (+3±7%). In the SoyFACE dataset, a statistically significant 15% reduction in SLA was observed for the developed leaves at the early growing stage, though the reduction was only 5% (statistically insignificant) at the mid-growing stage (Ainsworth et al., 2007). Ozone exposure has an opposing effect on SLA compared to elevated CO_2 concentrations. SoyFACE experiments observed a statistically significant increase in SLA by 10–22% at ozone concentrations of 190–200 ppb relative to ambient ozone concentrations for soybean (Fig. S4; Betzelberger et al., 2012), while the effect on maize SLA was insignificant (Choquette et al., 2020). With the implementation of varying SLA in response to changing CO_2 and O_3 concentrations, LAI is primarily modified through the change in SLA, as well as the diminished or amplified LAI-GPP feedback during the early- to mid-growing stage.

At late growing stages, LAI changes are mostly driven by senescence loss. Current implementation of leaf senescence rate in TEMIR and models such as CLM4.5 and JULES is based on phenological timing, which can be further improved by including cumulative ozone uptake and water stress. Water deficit triggers early senescence for maize as documented in the Manderscheid et al. (2014) dataset. Exposure to high ozone concentrations also induces early senescence in crops (Betzelberger et al., 2012). Future improvements to the parameterization of leaf senescence could draw on crop models such as DSSAT (Guarin et al., 2024), which incorporates the impacts of ozone on leaf senescence rate.

5.5 Comparison of ozone sensitivity parameters to published relative response functions

The sensitivity parameter $a_{\text{Lombardozzi}}$ can be directly compared to sensitivities of O_3-uptake-based relative response functions. These relative response functions are derived from regressions of response variables (e.g, A_{sat}, g_s, and crop yield) to cumulative

https://doi.org/10.5194/egusphere-2026-5958
Preprint. Discussion started: 3 November 2026
© Author(s) 2026. CC BY 4.0 License.

stomatal uptake of O_3. The calculation of the cumulative stomatal uptake of O_3 varies in different studies, such as the method to calculate the stomatal conductance and the time window when O_3 uptake is considered.

Table 5 summarizes the sensitivities of different response variables to cumulative ozone uptake calculated with different values of F_{crit}. Peng et al. (2020) derived relative response functions using a multiplicative stomatal conductance model adopted, for example, in CLRTAP (2023). Parameters of the multiplicative stomatal conductance model were specifically calibrated to field observations. The resulting sensitivity of the loss in relative A_{sat} calculated with the multiplicative stomatal model is about 20% lower than that derived in this study (F_{crit} = 6 nmol O_3 m^{-2} s^{-1}), in which stomatal conductance was calculated using the Ball-Berry formulation. Using different methods to calculate stomatal conductance does not change the conclusion that the relative loss of A_{sat} is more sensitive than that for biomass to ozone uptake. When comparing different maize ozone exposure experiments, a large difference in the sensitivity of A_{sat} reduction to ozone uptake is observed. At the same F_{crit} value of 0, the sensitivity of the loss of relative photosynthetic rate to ozone uptake for the experiment conducted by Bagard et al. (2015) is ~8 times larger than that of Singh et al. (2023), and ~3 times larger than that of Peng et al. (2020). Mills et al. (2018) used a sensitivity −0.007 mmol O_3^{-1} m^2 (F_{crit} = 3 nmol O_3 m^{-2} s^{-1}) for global relative yield loss assessment of maize, deriving from the uptake-based yield loss function for wheat and the relative sensitivity of the concentration-based metric M7 for maize relative to that for wheat. This yield-loss sensitivity value of −0.004 mmol O_3^{-1} m^2 is only about 10–20% of the yield-loss sensitivity derived from the Peng and Singh datasets.

There are currently two soybean ozone exposure experiments with available uptake-based relative response functions to the best of our knowledge. Zhang et al. (2017) reported a mean sensitivity of −0.033 mmol O_3^{-1} m^2 (F_{crit} = 6 nmol O_3 m^{-2} s^{-1}) for the relative reduction in grain yield for four Chinese soybean cultivars. Assuming the sensitivity of the relative loss in grain yield is similar to that of relative A_{sat}, like what is observed from the SoyFACE dataset, the mean sensitivity of the US cultivars is ~20% lower than that of Chinese cultivars. Considering the uncertainties attributed to the calculation of stomatal conductance and measurements of response variables, they have essentially the same sensitivity to ozone. Mills et al. (2018) similarly derived an uptake-based yield-loss response function for soybean based on the relative sensitivity concentration-based metric M7 for soybean to wheat. The resulting uptake-based sensitivity of −0.007 mmol O_3^{-1} m^2 is lower compared to both values derived from the SoyFACE dataset and the study of Zhang et al. (2017).

In land surface models, crops are lumped into one or several categories. Comparing ozone sensitivity parameters derived for generalized crop simulations to those specifically calibrated for maize and soybean, generalized crops are less sensitive to ozone than maize and soybean. The sensitivity of the loss in relative A_{sat} to ozone uptake for generalized crops in Li et al. (2024) is calibrated using a logarithmic function at F_{crit} = 0.5 nmol O_3 m^{-2} s^{-1}, which corresponds to values of $a_{Lombardozzi,An}$ between −0.03 and −0.06 mmol O_3^{-1} m^2 at relevant O_3 concentration levels. This value of $a_{Lombardozzi,An}$ derived in Li et al. (2024) is larger than those derived in this study for maize (−0.012 and −0.035 nmol O_3^{-1} m^2 at F_{crit} = 0) and soybean (−0.013 nmol O_3^{-1} m^2 at F_{crit} = 0).

https://doi.org/10.5194/egusphere-2026-5958
Preprint. Discussion started: 3 November 2026
© Author(s) 2026. CC BY 4.0 License.

Table 5. Summary of the relative response functions of maize and soybean to cumulative effective ozone uptake derived in this study and other studies.

Reference	Response variables	Relative response functions and F_{crit} in nmol O_3 m^{-2} s^{-1} &
Maize		
This study based on data from Singh et al. (2023)	A_{sat}	$1 - (0.012\pm0.006)(CUO_0)$ $1 - (0.124\pm0.029)(CUO_3)$
	g_s	$1 - (0.007\pm0.006)(CUO_0)$ $1 - (0.100\pm0.033)(CUO_3)$
	Total biomass*	$1 - (0.12\pm0.04)(CUO_3)$
	Grain yield*	$1 - (0.04\pm0.02)(CUO_3)$
This study, based on data from Peng et al. (2020)	A_{sat}	$1.1 - (0.035\pm0.009)\ (CUO_0)$ $1 - (0.085\pm0.013)(CUO_3)$ $0.93 - (0.161\pm0.022)(CUO_6)$
	g_s	$0.90 - (0.006\pm0.009)(CUO_0)$ $0.89 - (0.020\pm0.019)(CUO_3)$ $0.87 - (0.033\pm0.036)(CUO_6)$
	Above-ground BM*	$1 - (0.05\pm0.02)(CUO_3)$
	Grain yield*	$1 - (0.02\pm0.01)(CUO_3)$
Peng et al. (2020)[#]	A_{sat}	$1 - 0.129(CUO_6)$
	Total biomass	$1 - 0.053(CUO_6)$
	Above-ground BM	$1 - 0.051(CUO_6)$
Mills et al. (2018)	Grain yield	$1 - 0.004(CUO_3)$
Bagard et al. (2015)	A_n	$1 - 0.1(CUO_0)^{\wedge}$
Soybean		
This study, based on data from Betzelberger et al. (2012)	A_{sat}	$1 - (0.022\pm0.003)(CUO_4)$ $1 - (0.027\pm0.003)(CUO_6)$
	g_s	$1 - (0.020\pm0.005)(CUO_4)$ $1 - (0.024\pm0.005)(CUO_6)$
	Grain yield*	$1 - (0.022\pm0.005)(CUO_4)$
Zhang et al. (2017)	Grain yield	$1 - 0.033(CUO_6)$
Mills et al., (2018)	Grain yield	$1 - 0.007(CUO_3)$
Generalized crops		
Li et al. (2024)	A_n	$0.909 - 0.028\ln(CUO_{0.5})$
	g_s	$1 - 0.169\tanh(CUO_{0.5})$
Lombardozzi et al. (2015) 'Average sensitivity'	A_n	$0.8021 - 0.0009(CUO_{0.8})$
	g_s	0.7511

[#] Parameters directly retrieved from Peng et al. (2020), where stomatal conductance is calculated based on a multiplicative function (Jarvis, 1976) that is calibrated to leaf-level gas-exchange measurements, unlike the Ball-Berry formulation used in

https://doi.org/10.5194/egusphere-2026-5958
Preprint. Discussion started: 3 November 2026
© Author(s) 2026. CC BY 4.0 License.

TEMIR in this study. * The slope of the relative response function is based on inspections of Figure 8, Figure 10 and Figure 11, but not based on the regression slopes between target variables and CUO. & Regression intercepts are only specified if they deviate from 1 by more than 0.05. ^ By inspecting Figure 2D in Bagard et al. (2015)

6 Conclusions

A process-based crop module has been implemented into the Terrestrial Ecosystem Model in R (TEMIR), enabling simulations of crop carbon budgets, phenology, and physical structure at various CO_2 and surface ozone concentrations. Evaluated against eddy-covariance flux observations, the model reliably reproduces key ecosystem variables, such as GPP and biomass, for maize and soybean. Evaluated against elevated CO_2 fumigation experiments, TEMIR reproduces varying responses of C_3 and C_4 crops to high CO_2 concentrations for biomass and yield. Following the cumulative stomatal ozone uptake framework, two sets of plant-ozone damage parameters, one for each crop, are derived using relative gas-exchange rate loss observation data from ozone fumigation experiments. For soybean, using calibrated parameters, the model reproduces relative yield loss with a mean error of less than 5 percentage points, substantially improved from the default parameters (mean error of 30 percentage points). The small mean error arising from using the parameters calibrated from relative gas-exchange rate loss suggests that photosynthetic impairment closely mirrors yield declines in soybean. In contrast, such mirroring is not observed in maize, where crop yield displays buffering from ozone damage relative to gas-exchange rates. The ozone damage sensitivity parameter calibrated to photosynthetic rate loss has to be reduced by 66 – 75% to match harvest data. This differential sensitivity of plant physiology toward ozone underscores the importance of selecting appropriate ozone damage parameters according to the research goal, distinguishing between yield assessments, and carbon- and water-cycle assessments under ozone pollution.

As a computationally efficient offline model, the new TEMIR crop module facilitates multi-scale assessments of agricultural vulnerability under diverse climate and ozone pollution scenarios. Its compatible input structure with the chemical transport model GEOS-Chem provides a versatile platform to evaluate how land-use shifts, precursor emission controls, and climate interventions impact surface ozone concentrations, and thereby crop yield. Ultimately, this framework delivers science-based evidence on the agricultural co-benefits of air quality management, directly advancing climate-resilient food security and United Nations Sustainable Development Goals.

https://doi.org/10.5194/egusphere-2026-5958
Preprint. Discussion started: 3 November 2026
© Author(s) 2026. CC BY 4.0 License.

Code and data availability.

The Terrestrial Ecosystem Model in R (TEMIR) version 2.0 source code is free software licensed under the GNU General Public License v3 (GPL-3.0). The exact frozen version of the model code is archived on Zenodo at https://doi.org/10.5281/zenodo.23462305 (Pang and Tai, 2026a), with active development accessible on GitHub (https://github.com/yspang919/TEMIR). The input files required to run an example crop simulation in TEMIR v2.0 are archived on Zenodo at https://doi.org/10.5281/zenodo.21408341 (Pang and Tai, 2026b). Experimental data for the maize eCO_2 experiments (Manderscheid et al., 2014) are available through the Open Data Journal for Agricultural Research (https://doi.org/10.18174/odjar.v6i0.17915; Manderscheid et al., 2020). Observational data for the flux tower site IN-Hyd and maize ozone fumigation experiments (Peng et al., 2020) are uploaded to Zenodo at https://doi.org/10.5281/zenodo.23462820 (Pang et al., 2026). Experimental data for the Indian maize fumigation experiments (Singh et al., 2023) are available from the respective authors upon reasonable request.

Supplement.

……

Author contributions. JYSP led the study design, data analysis, and implemented the crop model. AAS and SBA contributed to the maize ozone exposure experiment data in India. SC contributed to the flux tower data at IN-Hyd. ZF contributed to the maize ozone exposure experiment data in China. APKT led the study design, funding acquisition, and developed the base TEMIR model. All authors have contributed to the writing of the manuscript.

Competing interests.

Amos P. K. Tai is a member of the EGU Editorial boards.

Acknowledgement.

We gratefully acknowledge the financial support of the Hong Kong Research Grants Council, and FLUXNET and AmeriFlux for the field data at the US-Ne2 sites. We thank Elizabeth Ainsworth and SoyFACE Team for the soybean ozone fumigation data.

Financial support.

Amos P. K. Tai has been supported by the Hong Kong Research Grants Council (Collaborative Research Fund no. C4028-24GF).

https://doi.org/10.5194/egusphere-2026-5958
Preprint. Discussion started: 3 November 2026
© Author(s) 2026. CC BY 4.0 License.

References

Ahmed, S., Raza, M. A., Zhou, T., Hussain, S., Khalid, M. H. B., Feng, L., Wasaya, A., Iqbal, N., Ahmed, A., Liu, W., and Yang, W.: Responses of Soybean Dry Matter Production, Phosphorus Accumulation, and Seed Yield to Sowing Time under Relay Intercropping with Maize, Agronomy, 8, 282, https://doi.org/10.3390/agronomy8120282, 2018.

Ainsworth, E. A. and Long, S. P.: What have we learned from 15 years of free-air CO_2 enrichment (FACE)? A meta-analytic review of the responses of photosynthesis, canopy properties and plant production to rising CO_2, New Phytol., 165, 351–372, https://doi.org/10.1111/j.1469-8137.2004.01224.x, 2005.

Ainsworth, E. A., Rogers, A., Leakey, A. D. B., Heady, L. E., Gibon, Y., Stitt, M., and Schurr, U.: Does elevated atmospheric [CO2] alter diurnal C uptake and the balance of C and N metabolites in growing and fully expanded soybean leaves?, J. Exp. Bot., 58, 579–591, https://doi.org/10.1093/jxb/erl233, 2007.

Aspray, E. K., Mies, T. A., McGrath, J. A., Montes, C. M., Dalsing, B., Puthuval, K. K., Whetten, A., Herriott, J., Li, S., Bernacchi, C. J., DeLucia, E. H., Leakey, A. D. B., Long, S. P., McGrath, J. M., Miglietta, F., Ort, D. R., and Ainsworth, E. A.: Two decades of fumigation data from the Soybean Free Air Concentration Enrichment facility, Sci Data, 10, 226, https://doi.org/10.1038/s41597-023-02118-x, 2023.

Avnery, S., Mauzerall, D. L., Liu, J., and Horowitz, L. W.: Global crop yield reductions due to surface ozone exposure: 2. Year 2030 potential crop production losses and economic damage under two scenarios of O3 pollution, Atmos. Environ., 45, 2297–2309, https://doi.org/10.1016/j.atmosenv.2011.01.002, 2011.

Bagard, M., Jolivet, Y., Hasenfratz-Sauder, M.-P., Gérard, J., Dizengremel, P., and Le Thiec, D.: Ozone exposure and flux-based response functions for photosynthetic traits in wheat, maize and poplar, Environ. Pollut., 206, 411–420, https://doi.org/10.1016/j.envpol.2015.07.046, 2015.

Bernacchi, C. J., Morgan, P. B., Ort, D. R., and Long, S. P.: The growth of soybean under free air [CO2] enrichment (FACE) stimulates photosynthesis while decreasing in vivo Rubisco capacity, Planta, 220, 434–446, https://doi.org/10.1007/s00425-004-1320-8, 2005.

Bernacchi, C. J., Leakey, A. D. B., Heady, L. E., Morgan, P. B., Dohleman, F. G., Mcgrath, J. M., Gillespie, K. M., Wittig, V. E., Rogers, A., Long, S. P., and Ort, D. R.: Hourly and seasonal variation in photosynthesis and stomatal conductance of soybean grown at future CO_2 and ozone concentrations for 3 years under fully open-air field conditions, Plant Cell Environ, 29, 2077–2090, https://doi.org/10.1111/j.1365-3040.2006.01581.x, 2006.

Betzelberger, A. M., Yendrek, C. R., Sun, J., Leisner, C. P., Nelson, R. L., Ort, D. R., and Ainsworth, E. A.: Ozone Exposure Response for U.S. Soybean Cultivars: Linear Reductions in Photosynthetic Potential, Biomass, and Yield, Plant Physiol., 160, 1827–1839, https://doi.org/10.1104/pp.112.205591, 2012.

Bhattarai, H., Tai, A. P. K., Val Martin, M., and Yung, D. H. Y.: Impacts of changes in climate, land use, and emissions on global ozone air quality by mid-21st century following selected Shared Socioeconomic Pathways, Sci. Total Environ., 906, 167759, https://doi.org/10.1016/j.scitotenv.2023.167759, 2024.

von Caemmerer, S. and Farquhar, G. D.: Some relationships between the biochemistry of photosynthesis and the gas exchange of leaves, Planta, 153, 376–387, https://doi.org/10.1007/BF00384257, 1981.

Cheesman, A. W., Brown, F., Artaxo, P., Farha, M. N., Folberth, G. A., Hayes, F. J., Heinrich, V. H. A., Hill, T. C., Mercado, L. M., Oliver, R. J., O' Sullivan, M., Uddling, J., Cernusak, L. A., and Sitch, S.: Reduced productivity and carbon

https://doi.org/10.5194/egusphere-2026-5958
Preprint. Discussion started: 3 November 2026
© Author(s) 2026. CC BY 4.0 License.

drawdown of tropical forests from ground-level ozone exposure, Nat. Geosci., 17, 1003–1007, https://doi.org/10.1038/s41561-024-01530-1, 2024.

Choquette, N. E., Ainsworth, E. A., Bezodis, W., and Cavanagh, A. P.: Ozone tolerant maize hybrids maintain Rubisco content and activity during long-term exposure in the field, Plant Cell Environ., 43, 3033–3047, https://doi.org/10.1111/pce.13876, 2020.

Clapp, R. B. and Hornberger, G. M.: Empirical equations for some soil hydraulic properties, Water Resour. Res., 14, 601–604, https://doi.org/10.1029/WR014i004p00601, 1978.

CLRTAP: Manual on Methodologies and Criteria for Modelling and Mapping Critical Loads and Levels and Air Pollution Effects, Risks, and Trends, German Environment Agency, 338 pp., https://doi.org/10.60810/openumwelt-6717, 2023.

Collatz, G. J., Ball, J. T., Grivet, C., and Berry, J. A.: Physiological and environmental regulation of stomatal conductance, photosynthesis and transpiration: a model that includes a laminar boundary layer, Agr. Forest Meteorol., 54, 107–136, https://doi.org/10.1016/0168-1923(91)90002-8, 1991.

Collatz, G., Ribas-Carbo, M., and Berry, J.: Coupled Photosynthesis-Stomatal Conductance Model for Leaves of C4 Plants, Functional Plant Biol., 19, 519, https://doi.org/10.1071/PP9920519, 1992.

Cosby, B. J., Hornberger, G. M., Clapp, R. B., and Ginn, T. R.: A Statistical Exploration of the Relationships of Soil Moisture Characteristics to the Physical Properties of Soils, Water Resour. Res., 20, 682–690, https://doi.org/10.1029/WR020i006p00682, 1984.

Dermody, O., Long, S. P., and DeLucia, E. H.: How does elevated CO_2 or ozone affect the leaf-area index of soybean when applied independently?, New Phytol., 169, 145–155, https://doi.org/10.1111/j.1469-8137.2005.01565.x, 2006.

Dickinson, R. E.: Land Surface Processes and Climate—Surface Albedos and Energy Balance, in: Advances in Geophysics, vol. 25, Elsevier, 305–353, https://doi.org/10.1016/S0065-2687(08)60176-4, 1983.

van Dijk, M., Morley, T., Rau, M. L., and Saghai, Y.: A meta-analysis of projected global food demand and population at risk of hunger for the period 2010–2050, Nat Food, 2, 494–501, https://doi.org/10.1038/s43016-021-00322-9, 2021.

Drewniak, B., Song, J., Prell, J., Kotamarthi, V. R., and Jacob, R.: Modeling agriculture in the Community Land Model, Geosci. Model Dev., 6, 495–515, https://doi.org/10.5194/gmd-6-495-2013, 2013.

FAO: The future of food and agriculture: trends and challenges, Food and Agriculture Organization of the United Nations, Rome, 163 pp., ISBN 978-92-5-109551-5, 2017.

Farquhar, G. D., von Caemmerer, S., and Berry, J. A.: A biochemical model of photosynthetic CO_2 assimilation in leaves of C3 species, Planta, 149, 78–90, https://doi.org/10.1007/BF00386231, 1980.

Feng, Z., Xu, Y., Kobayashi, K., Dai, L., Zhang, T., Agathokleous, E., Calatayud, V., Paoletti, E., Mukherjee, A., Agrawal, M., Park, R. J., Oak, Y. J., and Yue, X.: Ozone pollution threatens the production of major staple crops in East Asia, Nat Food, 3, 47–56, https://doi.org/10.1038/s43016-021-00422-6, 2022.

Franz, M. and Zaehle, S.: Competing effects of nitrogen deposition and ozone exposure on northern hemispheric terrestrial carbon uptake and storage, 1850–2099, Biogeosciences, 18, 3219–3241, https://doi.org/10.5194/bg-18-3219-2021, 2021.

https://doi.org/10.5194/egusphere-2026-5958
Preprint. Discussion started: 3 November 2026
© Author(s) 2026. CC BY 4.0 License.

Gaspar, A. P., Laboski, C. A. M., Naeve, S. L., and Conley, S. P.: Dry Matter and Nitrogen Uptake, Partitioning, and Removal across a Wide Range of Soybean Seed Yield Levels, Crop Science, 57, 2170–2182, https://doi.org/10.2135/cropsci2016.05.0322, 2017.

Gillespie, K. M., Xu, F., Richter, K. T., Mcgrath, J. M., Markelz, R. J. C., Ort, D. R., Leakey, A. D. B., and Ainsworth, E. A.: Greater antioxidant and respiratory metabolism in field-grown soybean exposed to elevated O_3 under both ambient and elevated CO_2, Plant Cell & Environment, 35, 169–184, https://doi.org/10.1111/j.1365-3040.2011.02427.x, 2012.

Global Modeling And Assimilation Office (GMAO): MERRA-2 tavg1_2d_lnd_Nx: 2d,1-Hourly,Time-Averaged,Single-Level,Assimilation,Land Surface Diagnostics V5.12.4, https://doi.org/10.5067/RKPHT8KC1Y1T, 2015.

Guarin, J. R., Jägermeyr, J., Ainsworth, E. A., Oliveira, F. A. A., Asseng, S., Boote, K., Elliott, J., Emberson, L., Foster, I., Hoogenboom, G., Kelly, D., Ruane, A. C., and Sharps, K.: Modeling the effects of tropospheric ozone on the growth and yield of global staple crops with DSSAT v4.8.0, Geosci. Model Dev., 17, 2547–2567, https://doi.org/10.5194/gmd-17-2547-2024, 2024.

Halvorson, A. D. and Johnson, J. M. F.: Corn Cob Characteristics in Irrigated Central Great Plains Studies, Agron. J., 101, 390–399, https://doi.org/10.2134/agronj2008.0142x, 2009.

Infante, P., Moore, K., Hurburgh, C., Scott, P., Archontoulis, S., Lenssen, A., and Fei, S.: Biomass Production and Composition of Temperate and Tropical Maize in Central Iowa, Agronomy, 8, 88, https://doi.org/10.3390/agronomy8060088, 2018.

Jarvis, P. G.: The interpretation of the variations in leaf water potential and stomatal conductance found in canopies in the field, Phil. Trans. R. Soc. Lond. B, 273, 593–610, https://doi.org/10.1098/rstb.1976.0035, 1976.

Karimindla, A. R., Kumari, S., S R, S., Chintala, S., and P. Kambhammettu, B.: The role of time averaging of eddy covariance fluxes on water use efficiency dynamics of maize, Atmos. Meas. Tech., 17, 5477–5490, https://doi.org/10.5194/amt-17-5477-2024, 2024.

Lawrence, D. M. and Slater, A. G.: Incorporating organic soil into a global climate model, Clim Dyn, 30, 145–160, https://doi.org/10.1007/s00382-007-0278-1, 2008.

Leung, F., Williams, K., Sitch, S., Tai, A. P. K., Wiltshire, A., Gornall, J., Ainsworth, E. A., Arkebauer, T., and Scoby, D.: Calibrating soybean parameters in JULES 5.0 from the US-Ne2/3 FLUXNET sites and the SoyFACE-O_3 experiment, Geosci. Model Dev., 13, 6201–6213, https://doi.org/10.5194/gmd-13-6201-2020, 2020.

Li, C., Gu, X., Wu, Z., Qin, T., Guo, L., Wang, T., Zhang, L., and Jiang, G.: Assessing the effects of elevated ozone on physiology, growth, yield and quality of soybean in the past 40 years: A meta-analysis, Ecotoxicol. Environ. Saf., 208, 111644, https://doi.org/10.1016/j.ecoenv.2020.111644, 2021.

Li, F., Zhou, Z., Levis, S., Sitch, S., Hayes, F., Feng, Z., Reich, P. B., Zhao, Z., and Zhou, Y.: Quantifying the role of ozone-caused damage to vegetation in the Earth system: a new parameterization scheme for photosynthetic and stomatal responses, Geosci. Model Dev., 17, 6173–6193, https://doi.org/10.5194/gmd-17-6173-2024, 2024.

Li, S., Moller, C. A., Mitchell, N. G., Lee, D., Sacks, E. J., and Ainsworth, E. A.: Testing unified theories for ozone response in C_4 species, Glob. Change Biol., 28, 3379–3393, https://doi.org/10.1111/gcb.16108, 2022.

https://doi.org/10.5194/egusphere-2026-5958
Preprint. Discussion started: 3 November 2026
© Author(s) 2026. CC BY 4.0 License.

Li, Z., Zhan, C., Hu, S., Ning, L., Wu, L., and Guo, H.: Implementation of a dynamic specific leaf area (SLA) into a land surface model (LSM) incorporated crop-growth model, Comput. Electron. Agr., 213, 108238, https://doi.org/10.1016/j.compag.2023.108238, 2023.

Lombardozzi, D., Sparks, J. P., Bonan, G., and Levis, S.: Ozone exposure causes a decoupling of conductance and photosynthesis: implications for the Ball-Berry stomatal conductance model, Oecologia, 169, 651–659, https://doi.org/10.1007/s00442-011-2242-3, 2012a.

Lombardozzi, D., Levis, S., Bonan, G., and Sparks, J. P.: Predicting photosynthesis and transpiration responses to ozone: decoupling modeled photosynthesis and stomatal conductance, Biogeosciences, 9, 3113–3130, https://doi.org/10.5194/bg-9-3113-2012, 2012b.

Lombardozzi, D., Sparks, J. P., and Bonan, G.: Integrating O_3 influences on terrestrial processes: photosynthetic and stomatal response data available for regional and global modeling, Biogeosciences, 10, 6815–6831, https://doi.org/10.5194/bg-10-6815-2013, 2013.

Lombardozzi, D., Levis, S., Bonan, G., Hess, P. G., and Sparks, J. P.: The Influence of Chronic Ozone Exposure on Global Carbon and Water Cycles, Journal of Climate, 28, 292–305, https://doi.org/10.1175/JCLI-D-14-00223.1, 2015.

Luo, X., Zhao, R., Chu, H., Collalti, A., Fatichi, S., Keenan, T. F., Lu, X., Nguyen, N., Prentice, I. C., Sun, W., Yu, K., and Yu, L.: Global variation in vegetation carbon use efficiency inferred from eddy covariance observations, Nat Ecol Evol, 9, 1414–1425, https://doi.org/10.1038/s41559-025-02753-0, 2025.

Lv, Z., Li, F., and Lu, G.: Adjusting sowing date and cultivar shift improve maize adaption to climate change in China, Mitig Adapt Strateg Glob Change, 25, 87–106, https://doi.org/10.1007/s11027-019-09861-w, 2020.

Manderscheid, R., Erbs, M., and Weigel, H.-J.: Interactive effects of free-air CO2 enrichment and drought stress on maize growth, Eur. J. Agron., 52, 11–21, https://doi.org/10.1016/j.eja.2011.12.007, 2014.

Manderscheid, R., Erbs, M., Kellner, J., Hüther, L., Kraft, P., Wieser, H., and Weigel, H.-J.: Maize response to free air CO2 enrichment under ample and restricted water supply: field experimental data and output of a process-based hydrological plant growth model, Open Data J. Agric. Res., 6, 34–38, https://doi.org/10.18174/odjar.v6i0.17915, 2020.

Mills, G., Sharps, K., Simpson, D., Pleijel, H., Frei, M., Burkey, K., Emberson, L., Uddling, J., Broberg, M., Feng, Z., Kobayashi, K., and Agrawal, M.: Closing the global ozone yield gap: Quantification and cobenefits for multistress tolerance, Glob. Change Biol., 24, 4869–4893, https://doi.org/10.1111/gcb.14381, 2018.

Moch, J. M., Mickley, L. J., Eastham, S. D., Lundgren, E. W., Shah, V., Buonocore, J. J., Pang, J. Y. S., Sadiq, M., and Tai, A. P. K.: Overlooked Long-Term Atmospheric Chemical Feedbacks Alter the Impact of Solar Geoengineering: Implications for Tropospheric Oxidative Capacity, AGU Advances, 4, e2023AV000911, https://doi.org/10.1029/2023AV000911, 2023.

Morgan, P. B., Ainsworth, E. A., and Long, S. P.: How does elevated ozone impact soybean? A meta-analysis of photosynthesis, growth and yield, Plant Cell Environ., 26, 1317–1328, https://doi.org/10.1046/j.0016-8025.2003.01056.x, 2003.

Mourtzinis, S., Specht, J. E., and Conley, S. P.: Defining Optimal Soybean Sowing Dates across the US, Sci Rep, 9, 2800, https://doi.org/10.1038/s41598-019-38971-3, 2019.

https://doi.org/10.5194/egusphere-2026-5958
Preprint. Discussion started: 3 November 2026
© Author(s) 2026. CC BY 4.0 License.

Murray, L. T., Leibensperger, E. M., Mickley, L. J., and Tai, A. P. K.: Estimating future climate change impacts on human mortality and crop yields via air pollution, Proc. Natl. Acad. Sci. U.S.A., 121, e2400117121, https://doi.org/10.1073/pnas.2400117121, 2024.

Oleson, K., Lawrence, D., Bonan, G., Drewniak, B., Huang, M., Koven, C., Levis, S., Li, F., Riley, W., Subin, Z., Swenson, S., Thornton, P., Bozbiyik, A., Fisher, R., Heald, C., Kluzek, E., Lamarque, J.-F., Lawrence, P., Leung, L., Lipscomb, W., Muszala, S., Ricciuto, D., Sacks, W., Sun, Y., Tang, J., and Yang, Z.-L.: Technical description of version 4.5 of the Community Land Model (CLM), NSF National Center for Atmospheric Research, https://doi.org/10.5065/D6RR1W7M, 2013.

Oliver, R. J., Mercado, L. M., Sitch, S., Simpson, D., Medlyn, B. E., Lin, Y.-S., and Folberth, G. A.: Large but decreasing effect of ozone on the European carbon sink, Biogeosciences, 15, 4245–4269, https://doi.org/10.5194/bg-15-4245-2018, 2018.

O'Neill, B. C., Kriegler, E., Ebi, K. L., Kemp-Benedict, E., Riahi, K., Rothman, D. S., Van Ruijven, B. J., Van Vuuren, D. P., Birkmann, J., Kok, K., Levy, M., and Solecki, W.: The roads ahead: Narratives for shared socioeconomic pathways describing world futures in the 21st century, Glob. Environ. Change, 42, 169–180, https://doi.org/10.1016/j.gloenvcha.2015.01.004, 2017.

Oo, A. Z., Yamamoto, A., Ono, K., Umamageswari, C., Mano, M., Vanitha, K., Elayakumar, P., Matsuura, S., Bama, K. S., Raju, M., Inubushi, K., Sudo, S., Saitoh, N., Hayashida, S., Ravi, V., and Ambethgar, V.: Ecosystem carbon dioxide exchange and water use efficiency in a triple-cropping rice paddy in Southern India: A two-year field observation, Sci. Total Environ., 854, 158541, https://doi.org/10.1016/j.scitotenv.2022.158541, 2023.

Osborne, T., Gornall, J., Hooker, J., Williams, K., Wiltshire, A., Betts, R., and Wheeler, T.: JULES-crop: a parametrisation of crops in the Joint UK Land Environment Simulator, Geosci. Model Dev., 8, 1139–1155, https://doi.org/10.5194/gmd-8-1139-2015, 2015.

Pang, J. Y. S., and Tai, A. P. K.: TEMIR v2.0 Public Release. Zenodo. https://doi.org/10.5281/zenodo.23462305, Zenodo, 2026a.

Pang, J. Y. S., and Tai, A. P. K.: TEMIR v2.0 Example case model input. Zenodo. https://doi.org/10.5281/zenodo.21408341, Zenodo, 2026b.

Pang, J. Y. S., Tai, A. P. K., Feng, Z., and Chintala, S.: TEMIR v2.0 model calibration observation data and modeling results. Zenodo. https://doi.org/10.5281/zenodo.23462820, 2026.

Pastorello, G., et al.: The FLUXNET2015 dataset and the ONEFlux processing pipeline for eddy covariance data, Sci Data, 7, 225, https://doi.org/10.1038/s41597-020-0534-3, 2020.

Peng, B., Guan, K., Chen, M., Lawrence, D. M., Pokhrel, Y., Suyker, A., Arkebauer, T., and Lu, Y.: Improving maize growth processes in the community land model: Implementation and evaluation, Agr. Forest Meteorol., 250–251, 64–89, https://doi.org/10.1016/j.agrformet.2017.11.012, 2018.

Peng, J., Shang, B., Xu, Y., Feng, Z., and Calatayud, V.: Effects of ozone on maize (Zea mays L.) photosynthetic physiology, biomass and yield components based on exposure- and flux-response relationships, Environ. Pollut., 256, 113466, https://doi.org/10.1016/j.envpol.2019.113466, 2020.

https://doi.org/10.5194/egusphere-2026-5958
Preprint. Discussion started: 3 November 2026
© Author(s) 2026. CC BY 4.0 License.

Penning de Vries, F. W. T., Jansen, D. M., ten Berge, H. F. M., and Bakema, A.: Simulation of ecophysiological processes of growth in several annual crops, Simulation Monographs 29, Pudoc, Wageningen, the Netherlands, 271 pp., ISBN 90-220-1000-7, 1989.

Pleijel, H., Danielsson, H., Ojanperä, K., Temmerman, L. D., Högy, P., Badiani, M., and Karlsson, P. E.: Relationships between ozone exposure and yield loss in European wheat and potato—a comparison of concentration- and flux-based exposure indices, Atmos. Environ., 38, 2259–2269, https://doi.org/10.1016/j.atmosenv.2003.09.076, 2004.

Reddy, K. N., Baidya Roy, S., Rabin, S. S., Lombardozzi, D. L., Varma, G. V., Biswas, R., and Naik, D. C.: Improving the representation of major Indian crops in the Community Land Model version 5.0 (CLM5) using site-scale crop data, Geosci. Model Dev., 18, 763–785, https://doi.org/10.5194/gmd-18-763-2025, 2025.

Reich, P. B.: Quantifying plant response to ozone: a unifying theory, Tree Physiology, 3, 63–91, https://doi.org/10.1093/treephys/3.1.63, 1987.

Rotundo, J. L., Tang, T., and Messina, C. D.: Response of maize photosynthesis to high temperature: Implications for modeling the impact of global warming, Plant Physiol. Bioch., 141, 202–205, https://doi.org/10.1016/j.plaphy.2019.05.035, 2019.

Ryan, M. G.: Effects of Climate Change on Plant Respiration, Ecol. Appl., 1, 157–167, https://doi.org/10.2307/1941808, 1991.

Sacks, W. J., Deryng, D., Foley, J. A., and Ramankutty, N.: Crop planting dates: an analysis of global patterns, Glob. Ecol. Biogeogr., 19, 607–620, https://doi.org/10.1111/j.1466-8238.2010.00551.x, 2010.

Sadiq, M., Tai, A. P. K., Lombardozzi, D., and Val Martin, M.: Effects of ozone–vegetation coupling on surface ozone air quality via biogeochemical and meteorological feedbacks, Atmos. Chem. Phys., 17, 3055–3066, https://doi.org/10.5194/acp-17-3055-2017, 2017.

Sampedro, J., Waldhoff, S. T., Van De Ven, D.-J., Pardo, G., Van Dingenen, R., Arto, I., Del Prado, A., and Sanz, M. J.: Future impacts of ozone driven damages on agricultural systems, Atmos. Environ., 231, 117538, https://doi.org/10.1016/j.atmosenv.2020.117538, 2020.

Sellers, P. J.: Canopy reflectance, photosynthesis and transpiration, Int. J. Remote Sens., 6, 1335–1372, https://doi.org/10.1080/01431168508948283, 1985.

Singh, A. A., Ghosh, A., Pandey, B., Agrawal, M., and Agrawal, S. B.: Unravelling the ozone toxicity in Zea mays L. (C4 plant) under the elevated level of CO2 fertilization, Trop Ecol, 64, 739–755, https://doi.org/10.1007/s42965-023-00298-6, 2023.

Sitch, S., Cox, P. M., Collins, W. J., and Huntingford, C.: Indirect radiative forcing of climate change through ozone effects on the land-carbon sink, Nature, 448, 791–794, https://doi.org/10.1038/nature06059, 2007.

Tai, A. P. K., Sadiq, M., Pang, J. Y. S., Yung, D. H. Y., and Feng, Z.: Impacts of Surface Ozone Pollution on Global Crop Yields: Comparing Different Ozone Exposure Metrics and Incorporating Co-effects of CO2, Front. Sustain. Food Syst., 5, 534616, https://doi.org/10.3389/fsufs.2021.534616, 2021.

Tai, A. P. K., Yung, D. H. Y., and Lam, T.: Terrestrial Ecosystem Model in R (TEMIR) version 1.0: simulating ecophysiological responses of vegetation to atmospheric chemical and meteorological changes, Geosci. Model Dev., 17, 3733–3764, https://doi.org/10.5194/gmd-17-3733-2024, 2024.

https://doi.org/10.5194/egusphere-2026-5958
Preprint. Discussion started: 3 November 2026
© Author(s) 2026. CC BY 4.0 License.

van Vuuren, D. P., Edmonds, J., Kainuma, M., Riahi, K., Thomson, A., Hibbard, K., Hurtt, G. C., Kram, T., Krey, V., Lamarque, J.-F., Masui, T., Meinshausen, M., Nakicenovic, N., Smith, S. J., and Rose, S. K.: The representative concentration pathways: an overview, Climatic Change, 109, 5–31, https://doi.org/10.1007/s10584-011-0148-z, 2011.

Williams, K., Gornall, J., Harper, A., Wiltshire, A., Hemming, D., Quaife, T., Arkebauer, T., and Scoby, D.: Evaluation of JULES-crop performance against site observations of irrigated maize from Mead, Nebraska, Geosci. Model Dev., 10, 1291–1320, https://doi.org/10.5194/gmd-10-1291-2017, 2017.

Wu, X., Vuichard, N., Ciais, P., Viovy, N., De Noblet-Ducoudré, N., Wang, X., Magliulo, V., Wattenbach, M., Vitale, L., Di Tommasi, P., Moors, E. J., Jans, W., Elbers, J., Ceschia, E., Tallec, T., Bernhofer, C., Grünwald, T., Moureaux, C., Manise, T., Ligne, A., Cellier, P., Loubet, B., Larmanou, E., and Ripoche, D.: ORCHIDEE-CROP (v0), a new process-based agro-land surface model: model description and evaluation over Europe, Geosci. Model Dev., 9, 857–873, https://doi.org/10.5194/gmd-9-857-2016, 2016.

Wutzler, T., Lucas-Moffat, A., Migliavacca, M., Knauer, J., Sickel, K., Šigut, L., Menzer, O., and Reichstein, M.: Basic and extensible post-processing of eddy covariance flux data with REddyProc, Biogeosciences, 15, 5015–5030, https://doi.org/10.5194/bg-15-5015-2018, 2018.

Yendrek, C. R., Tomaz, T., Montes, C. M., Cao, Y., Morse, A. M., Brown, P. J., McIntyre, L. M., Leakey, A. D. B., and Ainsworth, E. A.: High-Throughput Phenotyping of Maize Leaf Physiological and Biochemical Traits Using Hyperspectral Reflectance, Plant Physiol., 173, 614–626, https://doi.org/10.1104/pp.16.01447, 2017.

Young, P. J., Archibald, A. T., Bowman, K. W., Lamarque, J.-F., Naik, V., Stevenson, D. S., Tilmes, S., Voulgarakis, A., Wild, O., Bergmann, D., Cameron-Smith, P., Cionni, I., Collins, W. J., Dalsøren, S. B., Doherty, R. M., Eyring, V., Faluvegi, G., Horowitz, L. W., Josse, B., Lee, Y. H., MacKenzie, I. A., Nagashima, T., Plummer, D. A., Righi, M., Rumbold, S. T., Skeie, R. B., Shindell, D. T., Strode, S. A., Sudo, K., Szopa, S., and Zeng, G.: Pre-industrial to end 21st century projections of tropospheric ozone from the Atmospheric Chemistry and Climate Model Intercomparison Project (ACCMIP), Atmos. Chem. Phys., 13, 2063–2090, https://doi.org/10.5194/acp-13-2063-2013, 2013.

Zhang, W., Feng, Z., Wang, X., Liu, X., and Hu, E.: Quantification of ozone exposure- and stomatal uptake-yield response relationships for soybean in Northeast China, Sci. Total Environ., 599–600, 710–720, https://doi.org/10.1016/j.scitotenv.2017.04.231, 2017.

Zhou, H., Zhou, G., He, Q., Zhou, L., Ji, Y., and Zhou, M.: Environmental explanation of maize specific leaf area under varying water stress regimes, Environ. Exp. Bot., 171, 103932, https://doi.org/10.1016/j.envexpbot.2019.103932, 2020.

Zhou, S. S., Tai, A. P. K., Sun, S., Sadiq, M., Heald, C. L., and Geddes, J. A.: Coupling between surface ozone and leaf area index in a chemical transport model: strength of feedback and implications for ozone air quality and vegetation health, Atmos. Chem. Phys., 18, 14133–14148, https://doi.org/10.5194/acp-18-14133-2018, 2018.

Zhu, J., Tai, A. P. K., and Hung Lam Yim, S.: Effects of ozone–vegetation interactions on meteorology and air quality in China using a two-way coupled land–atmosphere model, Atmos. Chem. Phys., 22, 765–782, https://doi.org/10.5194/acp-22-765-2022, 2022.